



Published in final edited form as:

Cancer Discov. 2019 November ; 9(11): 1538–1555. doi:10.1158/2159-8290.CD-19-0189.

## CDK7 inhibition suppresses Castration-Resistant Prostate Cancer through MED1 inactivation

Reyaz ur Rasool<sup>1, #</sup>, Ramakrishnan Natesan<sup>1, #</sup>, Qu Deng<sup>1, #</sup>, Shweta Aras<sup>1</sup>, Priti Lal<sup>5</sup>, Samuel Sander Efron<sup>1</sup>, Erick Mitchell-Velasquez<sup>1</sup>, Jessica M. Posimo<sup>1</sup>, Shannon Carskadon<sup>2</sup>, Sylvan C. Baca<sup>3</sup>, Mark M. Pomerantz<sup>3</sup>, Javed Siddiqui<sup>4</sup>, Lauren E. Schwartz<sup>5</sup>, Daniel J. Lee<sup>6</sup>, Nallasivam Palanisamy<sup>2</sup>, Goutham Narla<sup>7</sup>, Robert B. Den<sup>8</sup>, Matthew L. Freedman<sup>3</sup>, Donita C. Brady<sup>1, 9</sup>, Irfan A. Asangani<sup>1, 9, 10, \*</sup>

<sup>1</sup>Department of Cancer Biology, Perelman School of Medicine, University of Pennsylvania.

<sup>2</sup>Department of Urology, Vattikuti Urology Institute, Henry Ford Health System, Detroit, MI 48202 USA

<sup>3</sup>Department of Medical Oncology, Dana-Farber Cancer Institute, Harvard Medical School, Boston, MA 02115, USA

<sup>4</sup>Department of Pathology, University of Michigan Medical School, Ann Arbor, MI 48109, USA.

<sup>5</sup>Department of Pathology, Perelman School of Medicine, University of Pennsylvania

<sup>6</sup>Department of Surgery, Perelman School of Medicine, University of Pennsylvania

<sup>7</sup>Division of Genetic Medicine, Department of Internal Medicine, University of Michigan, Ann Arbor, MI, USA

<sup>8</sup>Department of Radiation Oncology. Sidney Kimmel Medical College, Thomas Jefferson University, Philadelphia, Pennsylvania 19107, USA.

<sup>9</sup>Abramson Family Cancer Research Institute, Perelman School of Medicine, University of Pennsylvania.

**\*Corresponding Author:** Irfan A. Asangani, Ph.D., Assistant Professor, Department of Cancer Biology, Assistant Investigator, Abramson Family Cancer Research Institute, Core Member, Penn Epigenetics Institute, Perelman School of Medicine, University of Pennsylvania, 611 BRB II/III, 421 Curie Boulevard, Philadelphia, PA 19104-6160, Office: (215)746-8780 Lab: (215)746-8781, Fax: (215)573-6725, asangani@upenn.edu.

<sup>#</sup>shared first author

Authors' contributions

**Conception and design:** R. Rasool, R. Natesan, I.A. Asangani

**Development of methodology:** R. Rasool, R. Natesan, Q. Deng, I.A. Asangani

**Acquisition of data:** R. Rasool, R. Natesan, Q. Deng, S. Aras, S.S. Efron, E. Mitchell-Velasquez, J.M. Posimo, S. Carskadon, I.A. Asangani

**Analysis and interpretation of data:** R. Rasool, R. Natesan, Q. Deng, P. Lal, I.A. Asangani

**Writing, review, and/or revision of the manuscript:** R. Rasool, R. Natesan, I.A. Asangani

**Administrative, technical, or material support:** R. Natesan, S.C. Baca, M.M. Pomerantz, J. Siddiqui, L.E. Schwartz, D.J. Lee, N. Palanisamy, G. Narla, R.B. Den, M.L. Freedman, D.C. Brady, I.A. Asangani

**Study supervision:** I.A. Asangani

Data deposits

RNA-seq and ChIP-seq data have been deposited in the NCBI GEO database with the accession GSE125245.

**Conflict of interest:** None

<sup>10</sup>Epigenetics Institute, Perelman School of Medicine, University of Pennsylvania, Philadelphia, PA 19104, USA.

## Abstract

Metastatic castration-resistant prostate cancer (CRPC) is a fatal disease, primarily resulting from the transcriptional addiction driven by Androgen Receptor (AR). First-line CRPC treatments typically target AR-signaling, but are rapidly bypassed, resulting in only a modest survival benefit with the anti-androgens. Therapeutic approaches that more effectively block the AR-transcriptional axis are urgently needed. Here, we investigated the molecular mechanism underlying the association between the transcriptional co-activator MED1 and AR as a vulnerability in AR-driven CRPC. MED1 undergoes CDK7-dependent phosphorylation at T1457 and physically engages AR at super-enhancer sites, and is essential for AR-mediated transcription. Additionally, a CDK7 specific inhibitor THZ1 blunts AR-dependent neoplastic growth by blocking AR/MED1 co-recruitment genome-wide, as well as reverses the hyper-phosphorylated MED1 associated enzalutamide resistant phenotype. *In vivo*, THZ1 induces tumor regression of AR amplified castration-resistant human prostate cancer in xenograft mouse model. Together, we demonstrate that CDK7 inhibition selectively targets MED1-mediated, AR-dependent oncogenic transcriptional amplification, thus representing a potential new approach for the treatment of CRPC.

## Introduction

Prostate cancer (PCa) is the most common non-cutaneous malignancy and the second leading cause of cancer-related mortality in men of the western world (1). While effective surgical, radiation, and androgen ablation therapies exist for clinically localized prostate cancer, progression to metastatic castration-resistant prostate cancer (CRPC) is essentially incurable. The Androgen receptor (AR) is a major driver alteration in CRPC (2–4), and most prostate tumors remain addicted to AR-mediated transcription (5). Despite recent advances in anti-androgen therapy, 20–40% of patients with metastatic CRPC demonstrate *de novo* resistance to the FDA-approved drugs abiraterone and enzalutamide, and many of the responders acquire resistance resulting in a limited survival benefit (6–8). Therefore, the identification and therapeutic targeting of chromatin-associated co-activators or mediators of AR function should be considered as alternative or complementary strategies to block AR transcriptional addiction that defines a large majority of CRPC.

The evolutionarily conserved multi-subunit Mediator complex plays a central role in the regulation of gene transcription by virtue of its ability to functionally bridge gene-specific transcription factors with the RNA polymerase II-associated basal transcription machinery (9). MED1 (also known as TRAP220, PBP, and DRIP205) is a key component of the Mediator complex, and is responsible for targeting and anchoring the complex to both cell type-specific transcription factors and a broad range of nuclear receptors (NR), including AR (10). Despite its pivotal role in transcription, very little is known about the molecular determinants that regulate the formation of a functional MED1-AR complex. In this study, we deciphered that ligand-dependent AR transcriptional signaling is activated through a “phosphoswitch” catalyzed by cyclin-dependent-kinase 7 (CDK7). Specifically, CDK7

phosphorylates the transcriptional co-activator MED1 at threonine 1457 to promote the formation of the AR-transcriptional complex. Furthermore, inhibition of CDK7 with the recently developed covalent inhibitor THZ1 (11) attenuates AR-signaling and eliminates naïve as well as enzalutamide refractory AR-addicted PCa cells. Finally, THZ1 demonstrated *in vivo* efficacy in CRPC xenograft models, suggesting that the CDK7 inhibitors being tested in clinical trials for other malignancies could also be evaluated in refractory castration-resistant prostate cancer either as monotherapy or in combination with other targeted agents.

## Results

### Co-recruitment of AR and MED1 to the chromatin upon androgen stimulation

To systematically evaluate the significance of MED1 in establishing the ligand-dependent AR-*cistrome* and subsequent transcriptional amplification in PCa cells, we determined by ChIP-seq the genome-wide enrichment of MED1 and AR upon androgen (Dihydrotestosterone - DHT) stimulation in VCaP cells. We utilized VCaP cells, as this PCa cell line harbors AR genomic amplification found in greater than 85% of metastatic CRPC patients (4). As we reported previously (12), the average ChIP-seq signal for AR was highly enriched in DHT-treated cells, and this signal is significantly reversed with enzalutamide (Fig. 1a). Interestingly, MED1 also displayed increased chromatin association upon DHT stimulation, which was completely abolished by enzalutamide (Fig. 1a). This apparent trend may be attributed to the co-recruitment of AR and MED1 (Supplementary Fig. 1a) to 5,014 regions that are highly enriched in Androgen Responsive Elements (Supplementary Fig. 1b). To examine the nature of AR and MED1 bound sites, we first identified transcriptionally active regions using H3K27ac ChIP-seq in VCaP cells (13). H3K27ac was enriched at 93,004 regions, of which 37,974 were defined as enhancers, while 1,487 were characterized as super-enhancers (Fig. 1b). The latter refers to clusters of enhancers densely occupied by transcription factors, cofactors, and chromatin regulators and display a wide variety of chromatin modifications. Super-enhancers (SEs) have been found to play a significant role in the maintenance of cell-type specific gene expression patterns (14). Interestingly, these SE regions in VCaP cells are positioned within 100 kb of many AR-regulated coding genes and lncRNAs, including canonical AR targets such as *TMPRSS2*, *KLK3*, *ZBTB16*, *SLC45A3*, *PCAT1*, and *PRNCR1*, thus implicating these distal regulatory regions in AR transcriptional output. Our integrative analysis of H3K27ac, AR, and MED1 ChIP-seq data further exemplifies this point, wherein 92% of the SEs but only 43% of the enhancers, were enriched in AR (AR+H3K27ac), while more strikingly 65% of the SE, compared to 11% of the enhancers, are co-enriched for both AR and MED1 (AR+MED1+H3K27ac) (Fig. 1c). We also found AR and MED1 enrichment to be significantly higher in the 968 SE regions when compared to the 4136 enhancer regions (Fig. 1d). These observations together clearly establish that ligand-dependent AR activation results in robust co-recruitment of AR and MED1 to SEs, resulting in amplified expression of associated target genes, as exemplified by ChIP-seq tracks shown for *FKBP5* (Fig. 1e). We next analyzed AR ChIP-seq data from normal and primary prostate tumors (15) to ascertain whether AR recruitment to SEs is elevated during tumor development. While no considerable difference was observed in the genome-wide AR binding levels between the tumor and normal (Supplementary Fig. 1c), the

tumor tissues displayed a pronounced enrichment of AR in the SE regions (Fig. 1f). In addition, 70–90% of the AR+MED1+H3K27ac SE in VCaP, a cell line originally derived from vertebral metastasis, overlapped with AR enriched regions in primary tumors (Supplementary Fig. 1d–g). These data suggest that a large number of AR-bound SEs in the primary tumor may continue to be enlisted upon progression to metastasis *via* MED1 association to support SE/promoter long-range interactions required for transcriptional amplification.

Since AR and MED1 interactions are highly localized to the SE regions, we hypothesized that MED1 recruitment to AR-target gene loci is pivotal for AR-transcriptional activity and that modulation of MED1 expression or activity could provide a novel route to resolve AR-dependent transcriptional addiction in PCa. To test this hypothesis, we performed *MED1* knockdown in LNCaP and VCaP cells and observed a complete reversal of DHT-induced transcriptional changes without affecting AR expression (Supplementary Figs. 2a–d). Additionally, to address the effects of *MED1* depletion on SE associated genes, we attempted to integrate the ChIP-seq and RNA-seq data from VCaP cells. First, we analyzed and found that the magnitude of expression of genes (FPKM values from RNA-seq) associated with AR+MED1+H3K27ac containing enhancers and SEs were higher than that for the MED1+H3K27ac containing enhancers and SEs genes (Supplementary Fig. 2e). Second, we found a significantly higher expression of genes associated with AR +MED1+H3K27ac containing superenhancers compared to AR+MED1+H3K27ac enhancers ( $p < 1e-05$ ), suggesting that the MED1-AR interaction at SEs elicits much higher transcription of associated genes (Supplementary Fig. 2e). Third, *MED1* depletion led selective, significant decrease in the expression of genes associated with SEs containing AR +MED1+H3K27ac ( $p < 6e-133$ ), whereas genes marked with MED1+H3K27ac SE did not display any significant difference in expression ( $p < 1e-01$ ) (Supplementary Fig. 2e). Importantly, Gene set enrichment analysis (GSEA) (16) of the differentially expressed genes showed a highly significant negative enrichment of the Hallmark Androgen Response and growth associated transcriptional signatures (17) (Figs. 1g and Supplementary Fig. 2f). Together, these findings provide clear evidence for the integral role of MED1 in enhancer and SE associated AR target gene expression in prostate cancer.

### MED1 phosphorylation is required for its interaction with AR

Next, we investigated whether ligand-dependent AR activation leads to MED1 phosphorylation, which might promote its recruitment into the Mediator complex thereby facilitating chromatin binding (18). Using the Phos-tag immunoblot assay, in which the dinuclear metal complex (1,3-bis[bis(pyridin-2-ylmethyl)amino]propan-2-olato dizinc(II)) specifically binds to phosphorylated amino acids and generates a mobility shift on acrylamide gels proportional to the number of incorporated phosphates (19), we observed two additional slow migrating bands for MED1 in nuclear extracts from cells stimulated with DHT, compared to vehicle control, which were eliminated upon phosphatase (CIAP) treatment (Fig. 2a). Phosphorylation of Threonine1032 (T1032) and Threonine1457 (T1457) of MED1 has been shown to promote its association with RNA PolII and other Mediator subunits, inducing chromatin looping by increasing recruitment of transcription factors and co-activators on chromatin (18,20,21). We confirmed that the DHT-induced MED1

phosphorylation sites are indeed these two previously observed threonine residues by performing HA-pulldown followed by phospho-Threonine (p-Thr) immunoblotting and a Phos-tag assay in LNCaP cells overexpressing HA-tagged wild type, T1032A, T1457A or double mutant (DM) MED1 (Fig. 2b and 2c). Interestingly, Phos-tag analysis of the T1457A mutant displayed a complete loss of phosphorylation on T1032 (Fig. 2c) and both the T1457A and DM MED1 mutants showed impaired association with AR, suggesting that T1457 directed phosphorylation is a major step required for the assembly/stability of the AR-MED1 complex (Fig. 2b). Next, using the p-T1457 specific antibody that does not detect the T1457A mutant (Supplementary Fig. 3a), we observed a time-dependent increase in p-MED1 levels upon DHT stimulation with a concomitant increase in the expression of phosphoSer81-AR (p-AR), an active chromatin bound form of AR (22,23), suggesting a ligand-dependent phosphorylation of MED1 in AR positive PCa (Fig. 2d). In corroboration, treatment with AR degrader ARD-69 (24) led to the reduction in p-MED1 levels in a time-dependent manner in LNCaP cells (Supplementary Figure 3b). More importantly, post DHT stimulation, degradation of AR led to a concomitant loss in the p-MED1 levels and a subsequent shift of MED1 from the chromatin to the soluble nuclear fraction (Fig. 2e), clearly demonstrating the AR activation dependent MED1 phosphorylation recruit MED1 to the chromatin. In agreement, *AR* null LNCaP cells stimulated with DHT displayed no increase in p-MED1 levels (Supplementary Fig. 3c). Next, reciprocal immunoprecipitation for MED1 and AR confirmed their ligand-induced phosphorylation-dependent interaction as shown by the complete loss of interaction when nuclear lysates were treated with CIAP (Fig. 2f). Our findings that p-MED1 is a key regulator of AR transcription led us to reason that p-MED1 might also be associated with PCa progression defined by increased AR signaling. To test this hypothesis and access the feasibility of p-MED1 as a prognostic marker, we analyzed prostate cancer tissue microarrays (TMA) containing benign adjacent (n=48), primary (n=228) and metastatic (n=96) prostate tumor samples, and found a progressive increase in nuclear p-MED1 levels from benign, localized, and metastatic sites ( $p < 3 \times 10^{-12}$ ,  $p < 1 \times 10^{-15}$  and  $p < 4 \times 10^{-6}$ ) (Figs. 2g–h, and Supplementary Figs. 3d–e). These results agree with our *in vitro* findings and provide a molecular basis for the use of p-MED1 as both a prognostic marker for advanced prostate cancer and as a therapeutically targetable activator of AR signaling for the treatment of PCa.

### CDK7 directly phosphorylates MED1 at T1457

Next, to identify the kinase involved in the phosphorylation of MED1 in AR-driven PCa, we tested a series of transcriptional cyclin-dependent kinases (CDK), including CDK7, CDK9, CDK12 and CDK13 (25). We reasoned that transcriptional CDKs might be involved in MED1 phosphorylation as they have been previously shown to regulate processes associated with MED1 functions such as facilitation of gene-specific chromatin looping, coordination of chromatin modification events with pre-initiation complex assembly, and the regulation of transcriptional elongation by RNA PolII (21,25,26). We treated VCaP, LNCaP and 22RV1 mCRPC cell lines, all of which express AR but harbor three different clinically relevant AR structural variations, namely genomic copy-number amplification, gain-of-function mutation (T877A) and constitutively active splice variant (AR-v7), respectively, with a panel of CDK inhibitors (12,27). The pan-CDK inhibitor Dinaciclib completely abolished p-MED1 levels in all three tested cell lines grown in standard culture conditions (Fig. 3a). Contrary to



previous reports that suggest ERK involvement in MED1 phosphorylation (18), we found that MEK inhibition with trametinib did not result in loss of p-MED1. Treatment with THZ1, a novel highly specific covalent inhibitor of CDK7/12 and 13 reduced p-MED1 levels at baseline and when stimulated with DHT, while the CDK9 specific inhibitor LDC had no such effect on p-MED1 levels (11) (Fig. 3a and Supplementary Fig. 4a). THZ1 is a phenylaminopyrimidine bearing cysteine-reactive acrylamide moiety and unlike most CDK inhibitors identified before, the THZ1 targeting site on CDK7/12/13 lies outside the kinase domain, providing possible explanations for the increased specificity of inhibition. To identify the specific CDK responsible for the phosphorylation of MED1, using a mixture of four siRNAs, we performed knockdown of *CDK7*, *CDK12*, and *CDK13* individually, along with *CDK9* as a negative control. Interestingly, only *CDK7* knockdown led to the loss of DHT induced p-MED1 with a parallel reduction in prostate specific antigen (PSA) levels, that served as a direct readout of AR transcriptional activity (Fig. 3b and Supplementary Fig. 4b). The reduction in p-MED1 was further confirmed using individual siRNA against CDK7 as well as THZ1-R – a non-cysteine reactive analogue of THZ1 as a negative control (11) (Supplementary Fig. 4c). However, CDK7 rescue was able to restore the p-MED1 to the pre-knockdown levels (Fig. 3c). Additionally, mitogen induced p-MED1 was much strongly inhibited upon CDK7 knockdown, whereas knockdown of the previously reported MED1 kinase ERK (18) or AKT (20) displayed only a marginal reduction in the p-MED1 levels suggesting that these kinases could potentially be upstream effectors of CDK7 activity (Supplementary Fig. 4d). CDK7 is a serine/threonine kinase that shows a preference for a proline at the +1 position relative to the phosphoacceptor residue. The RNA PolII CTD heptad sequence repeat, 1-YSPSPS-7, in which CDK7 preferentially phosphorylates Ser5, obeys this rule (25,28,29). Additionally, CDK7 has been reported to phosphorylate sites containing Ser-Pro or Thr-Pro dipeptides within many DNA-binding transcription factors, including SPT5, E2F-1, Oct-1, and the tumor suppressor p53 (25). Interestingly, the evolutionarily conserved T1457 phosphoacceptor residue of MED1 located in its intrinsically disordered region (IDR), appears remarkably similar to the SPT5 site (30) (Supplementary Fig. 4e and 4f). We next sought to determine whether CDK7 can directly phosphorylate T1457 on MED1 by performing *in vitro* kinase assays. Using purified recombinant components of CDK-activating-complex (CAK) comprising CDK7, Cyclin H and MAT1, and recombinant GST-tagged MED1 protein (amino acid 1391–1490) we observed Threonine phosphorylation, specifically at T1457, which was completely inhibited by THZ1 (Fig. 3d). This was further confirmed by assessing the ability of CDK7 to phosphorylate a wildtype or T1457A mutant peptide. While CDK7-mediated phosphorylation of the T1457 wildtype peptide was inhibited by THZ1 treatment in a dose-dependent manner, CDK7 exhibited no activity towards the T1457A mutant peptide (Fig. 3e). CDK7 phosphorylation of T1457 was further confirmed by Phos-tag analysis where we observed the loss of slow migrating p-MED1 bands upon CDK7 inhibition by THZ1 or siRNA mediated knockdown (Supplementary Fig. 4g and 4h). Furthermore, VCaP and LNCaP cells showed a dose- and time-dependent decrease in MED1 p-T1457 levels that parallel reduced phosphorylation at Ser5 of RNA PolII upon THZ1 treatment (Supplementary Fig. 4i and 4j). Intriguingly, AR negative RWPE and DU145 cells demonstrated no such decrease in p-MED1 or pS5-PolII levels even at the highest tested concentration of THZ1 (Supplementary Fig. 4i). Reciprocal immunoprecipitation

experiments confirmed an endogenous association between MED1 and members of CDK-activating kinase (CAK) complex (25) along with RNA PolII and AR (Fig. 3f). Subsequently, we observed the loss of endogenous MED1–AR complex formation upon THZ1 treatment in VCaP and LNCaP cells (Fig. 3g). We next sought to address the functional significance of phosphorylation of T1457 towards chromatin binding and AR interaction. Compared to the THZ1 sensitive wildtype MED1, the chromatin fraction was devoid of the T1457A mutant, whereas the T1457D phosphomimic was not only found in the chromatin fraction but its association to chromatin was insensitive to THZ1 (Supplementary Fig. 5a). Notably, unlike wildtype MED1, the T1457D phosphomimic retained the interaction with AR in the presence of THZ1 (Fig. 3h). Furthermore, exogenous expression of phosphorylation mutants of MED1 after knockdown of endogenous *MED1*, demonstrated a reversal of the ligand-activated gene expression and cell proliferation by the T1457D phosphomimic, but not the T1457A mutant, even in the presence of THZ1 (Fig. 3i and Supplementary Figs. 5b–c). Lastly, compared to wildtype MED1, overexpression of T1457A displayed a dominant negative phenotype, whereas T1457D expression led to a further increase in the proliferation of LNCaP cells (Supplementary Fig. 5d). Together, these data identify MED1 T1457 as a novel substrate of CDK7 kinase and demonstrates its significance in AR signaling and PCa cell growth.

### **CDK7 inhibition by THZ1 leads to the reversal of ligand induced MED1 chromatin recruitment**

Next, to test whether inhibition of CDK7 would result in the loss of MED1 chromatin accessibility, we isolated cytoplasmic, nuclear and chromatin protein fractions from DHT-stimulated (6h) LNCaP cells, in the presence or absence of THZ1 (Fig. 4a). As expected, DHT-stimulation led to increased phosphorylation and recruitment of MED1 and AR to the chromatin from nuclear and cytoplasmic compartments, respectively, whereas THZ1 triggered a complete loss in the chromatin-bound levels of p-MED1/MED1 and confined the entire cellular fraction of MED1 to the nucleus (Fig. 4a). In contrast, the anti-androgen enzalutamide was unable to completely dissociate p-MED1 from the chromatin (Fig. 4a). These observations were further confirmed using ChIP-seq analysis of genome-wide MED1 and AR binding in VCaP and LNCaP cells. As expected, the average ChIP-seq signal for MED1 and AR was highly enriched in DHT-treated cells (Fig. 4b), and THZ1 entirely reversed the MED1 enrichment that in turn led to significant de-recruitment of AR genome-wide as a consequent disruption of MED1-AR complex in both VCaP and LNCaP cells. Examples of gene tracks of AR-specific genes co-occupied by MED1 and AR on upstream enhancers and SE corroborate the genome-wide findings (Fig. 4c). Next, focusing our evaluation specifically on the MED1 and AR bound regions (see Supplementary Fig. 6a), DHT stimulated VCaP cells displayed increased MED1 levels in the AR occupied enhancers and SEs, defined by H3K27ac, whereas enhancers and SEs devoid of AR but positive for MED1 did not show any such increase, further establishing ligand-dependent recruitment of MED1 to the AR bound regulatory regions (Fig. 4d). Notably, AR was enriched at a much higher level at both the enhancers and SEs co-occupied by MED1 (Supplementary Fig. 6b), suggesting the binding of MED1 following AR recruitment to the chromatin stabilizes the AR complex. As expected, THZ1 treated cells demonstrated more efficient loss of MED1 enrichment from the AR bound enhancers and SEs when compared to the AR-deficient

MED1 containing enhancers and SEs (Fig. 4d). Similar observations were made in the LNCaP cells (Supplementary Fig. 6c–e). Next, integration of the ChIP-seq data with RNA-seq transcriptome demonstrated that greater than 90% of DHT-induced genes common in VCaP and LNCaP cells were associated with AR and MED1 co-occupied enhancers and SEs (Fig. 4e). Interestingly, upon THZ1 treatment the SE associated genes displayed a significant reduction in expression ( $p < 7 \times 10^{-18}$ ) compared to enhancer-associated genes ( $p < 6 \times 10^{-14}$ ) (Fig. 4e). Additionally, GSEA analysis demonstrated a complete reversal in the expression of DHT-induced differentially expressed AR target genes upon THZ1 treatment in VCaP and LNCaP cells (Supplementary Figs. 6f–h). Next, we sought to compare the potency of THZ1 and enzalutamide in blocking DHT-induced AR target gene expression. LNCaP and VCaP cells were treated with THZ1 or enzalutamide followed by DHT treatment and analyzed for canonical AR target gene expression. THZ1, even at 100 nM, phenocopied the reduction in DHT-induced gene expression observed in the 10  $\mu$ M enzalutamide treatment condition (Supplementary Fig. 6i). We also performed *CDK7* knockdown to orthogonally validate the specificity of THZ1 in modulating AR transcriptional program and found a complete reversal of DHT-induced transcriptional changes, including loss of hallmark androgen response signature gene expression, without affecting AR protein expression (Supplementary Fig. 7a–d). Interestingly, the gene sets that were significantly affected by *CDK7* knockdown were analogous to those obtained by *MED1* knockdown (Supplementary Fig. 2d). These data establish the CDK7 inhibitor THZ1 as a potent agent for antagonizing AR-signaling through its ability to inhibit phosphorylation-dependent recruitment of MED1 to the AR *cistrome* in PCa cells.

### Prostate cancer cells with hyperactive AR-signaling are sensitive to CDK7 inhibition

Based on our observations that genetic and pharmacologic inhibition of CDK7 affected AR-signaling through the disruption of MED1-AR chromatin interaction (Fig. 3–4), we hypothesized that AR-dependent PCa cells would be more sensitive to THZ1 treatment. To test this hypothesis, we treated a panel of seven PCa lines and one benign prostate cell line with THZ1. Using a cell viability assay, we found that the five AR-dependent PCa lines tested were highly sensitive to THZ1 with a GI50 concentration ranging between 50–170 nM, whereas the remaining three AR-negative cells displayed a GI50 ranging from 400–600 nM (Fig. 5a). Interestingly, though all the cell lines expressed equal amounts of CDK7, AR-positive cells displayed higher p-MED1 levels (Fig. 5b). Additionally, even at a relatively low 50 nM concentration, THZ1 severely inhibited long-term colony formation of AR-positive cells (Fig. 5c and Supplementary Fig. 8a). Importantly, THZ1 treatment induced robust apoptosis in the AR-positive LNCaP and VCaP cells, a response not observed in the AR-negative PC3 and DU145 cells (Fig. 5d and 5e), suggesting that AR status as a major determinant of THZ1 sensitivity in PCa cells. Subsequently, treatment with THZ1 or siRNA knockdown of MED1 or CDK7 in LNCaP and VCaP cells decreased AR target protein expression, resulting in the induction of apoptosis, and preferential growth inhibition as compared to PC3 and DU145 cells (Supplementary Fig. 8b–e). To determine the effect of THZ1 on global transcription, we treated LNCaP, VCaP, and DU145 cells with 100 nM THZ1, a concentration at which substantial inhibition of MED1 phosphorylation was achieved (Supplementary Fig. 4), and performed gene expression profiling by RNA-seq. Reflecting the observed phenotypic response, treatment with THZ1 led to a massive change



in the gene expression in both the AR-positive VCaP and LNCaP cells, (1325 up/1203 down in VCaP and 2612 up/1695 down in LNCaP), whereas DU145 cells displayed minimal change in gene expression (191 up / 190 down) (Fig. 5f and Supplementary Fig. 9a). Gene Ontology terms for biological processes (GO:BP) for the 710 genes commonly down-regulated between VCaP and LNCaP strongly reiterates the dominant role of THZ1 in regulating key cellular processes, as shown by the enrichment for RNA PolII dependent transcription, cell cycle, DNA repair and chromatin organization (Fig. 5g). Moreover, GSEA in VCaP and LNCaP showed negative enrichment of the various hallmark signatures, including androgen response, MYC and E2F targets - known to be deregulated in AR-driven CRPC (31,32) (Fig. 5h, Supplementary Fig. 9b). Interestingly DU145 cells instead had positive enrichment for MYC and E2F target signatures (Supplementary Fig. 9c), which could explain the reduced sensitivity to THZ1 observed in AR-negative PCa cells. Furthermore, VCaP cells, which harbor the AR-responsive TMPRSS2-ERG gene fusion found in greater than 55% of PCa (33), displayed a negative enrichment of ERG signature and a reduction in ERG levels upon THZ1 treatment in a dose and time-dependent manner (Supplementary Fig. 9d–e). This efficient downregulation of ERG –an ETS family transcription factor is compelling as it is known to drive a unique transitional program, induce DNA damage, invasion and metastasis, and is difficult to target by small molecule inhibitors (34). Next, following a study that suggests direct phosphorylation of AR at S515 and transactivation by CDK7 kinase (35), we sought to address whether the observed downregulation of AR-signature by THZ1 is due to a reduction in the AR p-S515 levels. Unlike p-MED1, THZ1 treatment even at 200 nM for 12h did not reduce AR p-S515 levels (Supplementary Fig. 9f–g), suggesting the effects of THZ1 observed in AR signaling is primarily driven by its effect on p-MED1 and not on the presumed CDK7-mediated phosphorylation of AR at S515. However, the influence of THZ1 on AR phosphorylation at S515 via long-term treatment with THZ1 could not be ruled out. Together, these results disclose that THZ1 treatment of AR-positive cells directly interferes with AR and associated transcription factor activity *via* MED1 inactivation and inhibits key oncogenic pathways required for PCa survival.

### **Enzalutamide resistant PCa cells display higher levels of p-MED1 and are sensitive to THZ1**

One of the current first-line therapies for metastatic CRPC is enzalutamide, a second generation anti-androgen (36), to which resistance invariably develops (6,8). The major mechanism of acquired resistance to enzalutamide is restoration of AR-signaling, which presents challenges for long-term disease control (37). Therefore, we sought to investigate whether amplification of AR-signaling is mediated through CDK7-dependent MED1 phosphorylation in enzalutamide refractory PCa. Towards this, we first established resistant derivatives of LNCaP, LNCaP-AR, LAPC4 and VCaP cells by long-term exposure to enzalutamide. As expected, the enzalutamide-resistant cells displayed increased PSA expression suggestive of restored AR-signaling, surprisingly accompanied by increased p-MED1 levels (Fig. 6a). Additionally, compared to parental control, increased stability of MED1 was observed in enzalutamide-resistant cells resulting from its hyper-phosphorylated state (Fig. 6b). The increased AR stability observed in enzalutamide-resistant cells could be due to increased phosphorylation at S515 and S81 (23), and an indirect consequence of its

more stable binding to the p-MED1. Next, we sought to confirm the role of p-T1457 in MED1 stability by conducting additional cycloheximide chase experiments. As expected, compared to the wildtype T1457 MED1, the phospho-dead T1457A mutant protein demonstrated decreased stability and lower half-life (Fig. 6c). Pathologic phosphorylation results from both aberrant activation of kinases and inactivation of phosphatases and is a hallmark of many diseases including cancer. Protein phosphatase 2A (PP2A) is a heterotrimeric serine/threonine phosphatase that prevents pathogenic signaling by dephosphorylating substrates that are key signaling effectors. PP2A is a multi-protein complex that is minimally composed of a scaffolding A subunit (PP2A-A), a catalytic C subunit (PP2A-C) and a regulatory B subunit (PP2A-B). Substrate specificity is dictated by the binding of one of at least fifteen regulatory B subunits to form an active PP2A heterotrimer (38). PP2A inactivation has been associated with therapy resistance in multiple malignancies including CRPC (39). Though no change in CDK7 was observed, enzalutamide-resistant cells displayed significantly reduced PP2A (catalytic subunit) expression compared to their parental controls (Fig. 6a). Consistent with this cell line data, metastatic biopsies (brain and bone) from two enzalutamide refractory patients displayed increased p-MED1 with an associated loss in PP2A expression (Supplementary Fig. 10a). Knockdown of *PPP2CA*, the catalytic subunit of PP2A, which has been shown to significantly abrogate PP2A enzymatic activity, led to enhanced p-MED1 levels (Fig. 6d), confirming PP2A mediated regulation of MED1 phosphorylation. In support of these findings, treatment with THZ1 led to the loss of p-MED1, reduced PSA, increased apoptosis, and growth inhibition in enzalutamide resistant cells (Fig. 6e–f and Supplementary Fig. 10b). Together this data demonstrates that enzalutamide resistant cells with elevated levels of p-MED1 are highly susceptible to CDK7 inhibition due in part to restored AR-signaling and loss of PP2A.

### CDK7 inhibition by THZ1 blocks CRPC growth in mice

Based on our *in vitro* data identifying THZ1 as a potent inhibitor of AR-mediated transcription through MED1 inactivation (Fig. 3–5), we sought to study its efficacy in blocking castration-resistant prostate cancer growth in an *in vivo* mouse xenograft model. We utilized the VCaP model, as it harbors the *TMPRSS2:ERG* gene fusion and *AR* amplification, both of which are frequent molecular aberrations observed in CRPC patients (3). Although the VCaP cell line was originally derived from a patient with CRPC (40), these cells require constant androgen supplementation for *in vitro* growth. As a result of this phenomenon, the VCaP tumor xenograft responds to castration initially but eventually relapses in mouse models (12). VCaP tumor-bearing mice were established and then castrated, leading to tumor regression. Upon regrowth and once the tumors reached their original pre-castrated size (~150 mm<sup>3</sup>), mice were randomized into two groups and treated intraperitoneally with vehicle (n = 8) or THZ1 (10mg/kg/b.i.d.) (n = 8) for four weeks (Fig. 7a). Treatment with THZ1 led to a dramatic tumor regression compared to vehicle control (Fig. 7b and Supplementary Fig. 11a). Additionally, THZ1 treatment was well tolerated with no treatment-related systemic toxicity observed in mice (Supplementary Fig. 11b), suggesting that THZ1 treatment allows a broader therapeutic window in cancer versus normal cells. Tumors from vehicle-treated mice displayed higher PSA expression, a high proliferative activity and lower apoptosis (Fig. 7c and Supplementary Fig. 11c). By contrast,

the vast majority of the residual tumors from THZ1-treated animals demonstrated loss of PSA expression, necrosis, reduced proliferative activity and increased apoptosis. Importantly, there was a significant reduction in p-MED1 levels in THZ1 treated tumors confirming target engagement *in vivo*. The plasma PSA level in THZ1-treated mice was significantly reduced compared to vehicle treated mice (Fig. 7d), suggesting that THZ1 was able to potently inhibit AR-signaling *in vivo*. Interestingly, unlike the tumor regression phenotype observed for the VCaP xenografts, treatment with THZ1 at 10mg/kg b.i.d for four weeks led to tumor growth inhibition of AR-negative DU145 xenografts in the castrated mice (n = 8) (Supplementary Fig. 11d), which was associated with reduced p-MED1 levels, lower Ki-67 and increased apoptosis when compared to vehicle treated controls (Supplementary Figures 11d–g). Together, these data clearly demonstrate the *in vivo* efficacy of THZ1 in prostate cancer xenograft models. Additionally, the more marked effect of CDK7 inhibition in the castration-resistant VCaP xenograft model compared to the AR-negative DU145 model supports the *in vitro* results showing increased dependence in AR-driven tumors.

## Discussion

Maintenance of AR-signaling is the most frequent resistance mechanism in CRPC patients that develops after conventional hormone deprivation and newer generation anti-androgen therapies (41). Genetic and epigenetic events lead to AR amplification, mutation, and alternative splicing resulting in the observed AR-driven transcriptional addiction seen in CRPC (11). Here, we demonstrate that the CDK7 directed MED1 phosphorylation at T1457 is a key regulator of AR function, and inhibition of the CDK7-MED1 axis results in significant tumor growth inhibition in AR-positive prostate cancer cells in both cell culture and *in vivo* models. In addition to blocking AR-signaling and ligand-activated MED1 recruitment to chromatin, THZ1 also negatively regulates the expression and oncogenic activity of *TMPRSS2-ETS* gene fusion products. This is very exciting as the oncogenic ETS transcription factors have been notoriously difficult to target therapeutically (34). Collectively, this data suggests a model in which CDK7 inhibition simultaneously blocks the functional activity and/or expression of multiple oncogenic transcriptional drivers in prostate cancer including AR, ETS, MYC, and E2F, all of which require MED1 as a cofactor. Moreover, our data elucidating ligand-activated phosphorylation of MED1 by CDK7 and its recruitment to the AR bound SEs support the recent studies that revealed the phase-separation property of MED1 through its IDRs that result in the formation of high-density assembly of transcription apparatus at SEs (42,43). The mechanistic basis for the phase-separation of MED1 is not well understood, and we hypothesize that this may be due to the phosphorylation of MED1 by CDK7 in response to growth stimuli or nuclear translocation of steroid hormone receptors, such as AR. Additional structural, biophysical, and *in cellulo* phase-separation studies will be needed to test this hypothesis.

CDK7 is a ubiquitously expressed kinase (Supplementary Fig. 12a) that contributes to control of the cell cycle through phosphorylation of other CDKs, and plays a crucial role in transcription as part of the transcription factor TFIIF complex (44). A Pan-Cancer analysis for CDK7 in TCGA revealed comparable level expression (Supplementary Fig. 12b). However, little is known about CDK7 expression and activity in advanced prostate cancer.

Analysis of data sets comprising benign, primary, and metastatic prostate cancer showed no significant change in the expression of CDK7 mRNA between the groups (Supplementary Fig. 12c) which is in line with equal CDK7 protein levels observed in benign and PCa cells (Fig. 5b). Nevertheless, potential increase in CDK7 activity through T-loop Thr170 phosphorylation (45) by dysregulated MAPK and PI3K/AKT pathway in advanced prostate cancer cells could not be ruled out.

CDK7 inhibitors have demonstrated efficacy in T-cell acute lymphoblastic leukemia, small cell lung cancer, glioblastoma, and triple-negative breast cancer (11,46–48). The mechanism for the observed anti-tumor activity of CDK7 specific inhibitors is suggested to be the attenuation of transcriptional addiction required for the growth and survival of cancer cells. Though CDK7 is involved in normal transcription as an essential component of TFIIF (25), it is not clear why normal cells are less sensitive to CDK7 inhibition. One possible explanation is that cancer cells are addicted to transcription driven by SEs and thus highly dependent on CDK7 activity as exemplified by the identification of a so-called “Achilles cluster” of genes in TNBC, as well as MYCN amplified glioblastoma (46,48). These observations have led to the clinical development of CDK7 specific inhibitors. Currently, SY1365, a covalent CDK7 selective inhibitor is being assessed in a phase I trial in adult patients with advanced solid cancer as a single agent or in combination with standard of care therapies (<https://clinicaltrials.gov/ct2/show/NCT03134638>). Additionally, a second inhibitor, CT7001 (Carrick therapeutics, UK) is also in Phase I expansion for multiple malignancies.

While there has been much excitement around the development and successful clinical implementation of second-generation therapeutics targeting the androgen axis, such as abiraterone (7,49,50) and enzalutamide (8,51), the responses to these agents are often not durable. Resistance mechanisms to these drugs include those that develop with conventional hormonal treatment (e.g., AR amplification/ mutation/ intratumor androgen synthesis) as well as novel mechanisms involving compensatory steroid hormone signaling (e.g., estrogen receptor (ER) or glucocorticoid receptor (GR)) (41,52,53). As CDK7 inhibition functions “downstream” of AR itself through MED1 inactivation (Fig. 7e), our data suggest that CDK7 directed therapies may be effective in the context of a wide range AR-directed resistance mechanisms (54,55). Our identification of MED1 T1457 as a novel CDK7 substrate, which is essential for driving AR-mediated transcription makes CDK7 a potential “non-oncogene dependency” in advanced prostate cancer. Taken together, the data presented here strongly support the clinical evaluation of CDK7 specific inhibitors as a monotherapy or in combination with second generation anti-androgens in refractory CRPC.

## Methods

See supplementary materials for additional methods and Supplementary Table S1–S3 for the RNAseq, ChIPseq libraries and complete list of reagents.

## Cell Culture

Prostate parental cell lines used in this study were obtained from ATCC, LNCaP-AR cells were a gift from Dr. Charles Sawyers (Memorial Sloan-Kettering Cancer Center, New York,

NY), and LNCaP AR-KO cells were a gift from Dr. Dean Tang (Roswell Park Cancer Institute, Buffalo, NY) (56). LNCaP, LNCaP-AR, 22RV1, LAPC4, DU145, PC3, and LNCaP AR-KO prostate cancer cell lines were grown in RPMI 1640 (Gibco, 11875093), and VCaP prostate cancer cell line was grown in DMEM with Glutamax (Gibco, 21013024). The medium was supplemented with 10% of Fetal Bovine Serum (FBS) (HYC, SH30910.03) and 1% of Penicillin Streptomycin Solution (Invitrogen, 15140122), hereto referred to as “complete media”. The immortalized benign prostate cell line RWPE-1 was grown in keratinocyte media with supplements (Thermo Fisher Scientific, 17005042). LNCaP-AR and VCaP enzalutamide-resistant cell lines were derived from enzalutamide-resistant PCa tumor xenograft as described previously (57). LNCaP and LAPC4 enzalutamide-resistant cell lines were generated by culturing the cells in presence of 20  $\mu$ M enzalutamide for 3–4 months in vitro. Polyclonal pools of enzalutamide-resistant cells were cultured and maintained in media containing enzalutamide throughout. All experiments for enzalutamide resistant pools were done in presence of enzalutamide throughout the remainder of all experiments with these cells. The cell lines were tested negative for mycoplasma contamination and maintained in a humidified incubator at 37°C and 5% CO<sub>2</sub>.

**Drugs/chemicals:** CDK7 inhibitor-THZ1 (MedChem Express, HY-80013A/CS-3168), THZ1R (MedChem Express, HY-19988), LDC000067 (Selleckchem, S7461), Trametinib (Selleckchem, S2673), Enzalutamide (Selleckchem, S1250), Dinaciclib (Selleckchem, S2768), and PROTAC-ARD-69 (Gift from Dr. Shaomeng Wang @ U.Mich) (24) were dissolved and aliquoted in DMSO (Sigma-Aldrich, D2650). 5 $\alpha$ -Dihydrotestosterone (Cerilliant, D073) was dissolved and aliquoted in methanol. EGF (Thermo Fisher Scientific, PHG0311L) was dissolved in water.

### Phos-tag SDS-PAGE

The electrophoretic mobility shift in phosphorylated proteins was studied by following the Manganese (II)-Phos-tag SDS-PAGE (FUJIFILM Wako Pure Chemical Corporation, 30493521) method as described previously (58). Following the specific treatment, the cells were subjected to lysate preparation and analyzed through Phos-tag SDS PAGE (see Supplementary methods). Briefly, a 3.5% (wt/vol) separating gel solution containing 50  $\mu$ M polyacrylamide-bound Mn<sup>2+</sup>-Phos-tag and 0.5% (wt/vol) agarose and a stacking gel solution of 3.5% (wt/vol) containing 0.5% (wt/vol) agarose was prepared. The gel was run under constant-current conditions at room temperature for 3–4h. Upon completion of the run the gel was removed and soaked in 100 ml of blotting buffer containing 1 mM EDTA for 10 min. Wet tank transfer apparatus equipment was used to transfer the proteins on PVDF.

### Site directed mutagenesis

pWZL hygro Flag-HA TRAP220 wt plasmid was purchased from Addgene (plasmid,17433) and used for site-directed mutagenesis. Primers were designed, and site-directed mutagenesis was performed by the Quick-change II XL site-directed Mutagenesis Kit (Agilent Technologies, 200521). Three single mutants with point mutations T1032A, T1457A and T1457D as well as a double mutant containing T1032A and T1457A mutations were generated, using the manufacturer’s protocol. All plasmids were verified by DNA sequencing.



Primers used for mutagenesis are:

MED1 (T1032A) Fwd 5' – GTT CTT CTA ACA GAC CTT TTG CCC CAC CTA CCA  
GTA C -3'

MED1 (T1032A) Rev 5' – GTA CTG GTA GGT GGG GCA AAA GGT CTG TTA GAA  
GAA C -3'

MED1 (T1457A) Fwd 5' – GCC ATA GTA AGT CAC CAG CAT ATG CCC CCC AGA  
ATC TG -3'

MED1 (T1457A) Rev 5' – CAG ATT CTG GGG GGC ATA TGC TGG TGA CTT ACT  
ATG GC -3'

MED1 (T1457D) Fwd 5' – GCC ATA GTA AGT CAC CAG CAT ATG ACC CCC AGA  
ATC TG -3'

MED1 (T1457D) Rev 5' – CAG ATT CTG GGG GTC ATA TGC TGG TGA CTT ACT  
ATG GC -3'

### Chromatin immunoprecipitation (ChIP) and ChIP-seq

For ChIP-seq experiments, LNCaP and VCaP cells were grown in CSS containing media for 72h, followed by stimulation with 10 nM DHT in presence/absence of 100 nM THZ1 (6h treatment) or 10  $\mu$ M Enzalutamide (12h treatment). ChIP was performed using iDeal ChIP-seq Kit for Transcription Factors (Diagenode, C01010170) according to manufacturer's protocol. In brief, the cells were crosslinked with 1% formaldehyde in culture medium for 10 min at room temperature. Cross-linking was terminated by the addition of 1/10 volume 1.25 M glycine for 5 min at room temperature followed by cell lysis and sonication (Bioruptor, Diagenode), resulting in an average chromatin fragment size of 200 bp. Chromatin equivalent to  $5 \times 10^6$  cells was isolated and incubated with 10  $\mu$ g antibody overnight at 4 °C (MED1, H3-acetyl K27, AR, and IgG (Diagenode)). ChIP-seq libraries (Supplementary Table S2) were prepared from the ChIP-enriched DNA samples using the TruSeq ChIP Library Preparation Kit (Illumina, IP-202–1012, IP-202–1024) and protocol. In brief, ChIP-enriched DNA (1–10 ng) was converted to blunt-ended fragments. A single A-base was added to fragment ends followed by ligation of Illumina adaptors. The adaptor-modified DNA fragments were enriched by PCR using the Illumina Barcode primers and Phusion DNA polymerase. PCR products were size selected using 3% NuSieve agarose gels (Lonza) followed by gel extraction using QIAEX II reagents (QIAGEN). Libraries were quantified with the Bioanalyzer 2100 (Agilent) and sequenced on the Illumina NextSeq 500 Sequencer (75 nucleotide read length).

### Murine Prostate Tumor Xenograft Model

*In vivo* efficacy studies were performed in accordance with protocols approved by the Institutional Animal Care and Use Committee (IACUC) at the University of Pennsylvania and in compliance with all regulatory standards. Four to five-week-old male NOD SCID gamma mice (Jackson Lab, 005557) were procured from Jackson Laboratory. In the VCaP

experiment,  $2 \times 10^6$  VCaP prostate cancer cells suspended in 80  $\mu$ L of RPMI-1640 with 50% Matrigel (BD Biosciences) were implanted subcutaneously into the dorsal flank of the mice. The animals were castrated when the tumor volumes reached approximately 150 mm<sup>3</sup>. After castration, once the tumor relapsed to 150 mm<sup>3</sup>, mice were randomized into two groups, treated with either 10 mg/kg body weight THZ1 or 10% of DMSO in vehicle (D5W) intraperitoneally b.i.d for 4 weeks. In the DU145 xenograft experiments, animals were castrated one week before the subcutaneous implantation of DU145 ( $2 \times 10^6$ ) cells. Treatments of THZ1 at 10mg/kg or 10% of DMSO in vehicle (D5W) b.i.d started for 4 weeks when the tumors reached 150 mm<sup>3</sup>. Tumor growth in all studies was recorded using digital calipers and tumor volumes were estimated using the formula  $(\pi/6) (L \times W^2)$ , where L = length and W = width of tumor. Body weight during the study was also monitored. At the end of the treatment regimen the mice were sacrificed and were extracted for further analysis.

## Supplementary Material

Refer to Web version on PubMed Central for supplementary material.

## Acknowledgments

We thank Drs. A. Chinnaiyan and S. Wang from U.Mich for the reagent support. Research in I.A. Asangani laboratory is funded by Department of Defense Idea Development Award (W81XWH-17-1-0404 to I.A.A). J.M.P is supported by American Cancer Society Postdoctoral Fellowship 131203PF1714701CCG.

## References

1. Torre LA, Siegel RL, Ward EM, Jemal A. Global Cancer Incidence and Mortality Rates and Trends--An Update. *Cancer Epidemiol Biomarkers Prev* 2016;25(1):16–27 doi 10.1158/1055-9965.EPI-15-0578. [PubMed: 26667886]
2. Chen CD, Welsbie DS, Tran C, Baek SH, Chen R, Vessella R, et al. Molecular determinants of resistance to antiandrogen therapy. *Nat Med* 2004;10(1):33–9 doi 10.1038/nm972 nm972 [pii]. [PubMed: 14702632]
3. Robinson D, Van Allen EM, Wu YM, Schultz N, Lonigro RJ, Mosquera JM, et al. Integrative clinical genomics of advanced prostate cancer. *Cell* 2015;161(5):1215–28 doi 10.1016/j.cell.2015.05.001. [PubMed: 26000489]
4. Viswanathan SR, Ha G, Hoff AM, Wala JA, Carrot-Zhang J, Whelan CW, et al. Structural Alterations Driving Castration-Resistant Prostate Cancer Revealed by Linked-Read Genome Sequencing. *Cell* 2018;174(2):433–47 e19 doi 10.1016/j.cell.2018.05.036. [PubMed: 29909985]
5. Attard G, Cooper CS, de Bono JS. Steroid hormone receptors in prostate cancer: a hard habit to break? *Cancer Cell* 2009;16(6):458–62 doi 10.1016/j.ccr.2009.11.006. [PubMed: 19962664]
6. Antonarakis ES, Lu C, Wang H, Luber B, Nakazawa M, Roeser JC, et al. AR-V7 and resistance to enzalutamide and abiraterone in prostate cancer. *N Engl J Med* 2014;371(11):1028–38 doi 10.1056/NEJMoa1315815. [PubMed: 25184630]
7. de Bono JS, Logothetis CJ, Molina A, Fizazi K, North S, Chu L, et al. Abiraterone and increased survival in metastatic prostate cancer. *N Engl J Med* 2011;364(21):1995–2005 doi 10.1056/NEJMoa1014618. [PubMed: 21612468]
8. Scher HI, Fizazi K, Saad F, Taplin ME, Sternberg CN, Miller K, et al. Increased survival with enzalutamide in prostate cancer after chemotherapy. *N Engl J Med* 2012;367(13):1187–97 doi 10.1056/NEJMoa1207506. [PubMed: 22894553]
9. Allen BL, Taatjes DJ. The Mediator complex: a central integrator of transcription. *Nat Rev Mol Cell Biol* 2015;16(3):155–66 doi 10.1038/nrm3951. [PubMed: 25693131]

10. Chen W, Roeder RG. Mediator-dependent nuclear receptor function. *Semin Cell Dev Biol* 2011;22(7):749–58 doi 10.1016/j.semcdb.2011.07.026. [PubMed: 21854863]
11. Kwiatkowski N, Zhang T, Rahl PB, Abraham BJ, Reddy J, Ficarro SB, et al. Targeting transcription regulation in cancer with a covalent CDK7 inhibitor. *Nature* 2014;511(7511):616–20 doi 10.1038/nature13393. [PubMed: 25043025]
12. Asangani IA, Dommeti VL, Wang X, Malik R, Cieslik M, Yang R, et al. Therapeutic targeting of BET bromodomain proteins in castration-resistant prostate cancer. *Nature* 2014;510(7504):278–82 doi 10.1038/nature13229 nature13229 [pii]. [PubMed: 24759320]
13. Kron KJ, Murison A, Zhou S, Huang V, Yamaguchi TN, Shiah YJ, et al. TMPRSS2-ERG fusion co-opts master transcription factors and activates NOTCH signaling in primary prostate cancer. *Nat Genet* 2017;49(9):1336–45 doi 10.1038/ng.3930. [PubMed: 28783165]
14. Hnisz D, Abraham BJ, Lee TI, Lau A, Saint-Andre V, Sigova AA, et al. Super-enhancers in the control of cell identity and disease. *Cell* 2013;155(4):934–47 doi 10.1016/j.cell.2013.09.053. [PubMed: 24119843]
15. Pomerantz MM, Li F, Takeda DY, Lenci R, Chonkar A, Chabot M, et al. The androgen receptor cistrome is extensively reprogrammed in human prostate tumorigenesis. *Nat Genet* 2015;47(11):1346–51 doi 10.1038/ng.3419. [PubMed: 26457646]
16. Subramanian A, Tamayo P, Mootha VK, Mukherjee S, Ebert BL, Gillette MA, et al. Gene set enrichment analysis: a knowledge-based approach for interpreting genome-wide expression profiles. *Proc Natl Acad Sci U S A* 2005;102(43):15545–50 doi 10.1073/pnas.0506580102. [PubMed: 16199517]
17. Liberzon A, Birger C, Thorvaldsdóttir H, Ghandi M, Mesirov JP, Tamayo P. The Molecular Signatures Database (MSigDB) hallmark gene set collection. *Cell Syst* 2015;1(6):417–25 doi 10.1016/j.cels.2015.12.004. [PubMed: 26771021]
18. Belakavadi M, Pandey PK, Vijayvargia R, Fondell JD. MED1 phosphorylation promotes its association with mediator: implications for nuclear receptor signaling. *Mol Cell Biol* 2008;28(12):3932–42 doi 10.1128/MCB.02191-07. [PubMed: 18391015]
19. Kinoshita E, Kinoshita-Kikuta E, Takiyama K, Koike T. Phosphate-binding tag, a new tool to visualize phosphorylated proteins. *Mol Cell Proteomics* 2006;5(4):749–57 doi 10.1074/mcp.T500024-MCP200. [PubMed: 16340016]
20. Chen Z, Zhang C, Wu D, Chen H, Rorick A, Zhang X, et al. Phospho-MED1-enhanced UBE2C locus looping drives castration-resistant prostate cancer growth. *EMBO J* 2011;30(12):2405–19 doi 10.1038/emboj.2011.154. [PubMed: 21556051]
21. Fondell JD. The Mediator complex in thyroid hormone receptor action. *Biochim Biophys Acta* 2013;1830(7):3867–75 doi 10.1016/j.bbagen.2012.02.012. [PubMed: 22402254]
22. Chen S, Gulla S, Cai C, Balk SP. Androgen receptor serine 81 phosphorylation mediates chromatin binding and transcriptional activation. *J Biol Chem* 2012;287(11):8571–83 doi 10.1074/jbc.M111.325290. [PubMed: 22275373]
23. Pawar A, Gollavilli PN, Wang S, Asangani IA. Resistance to BET Inhibitor Leads to Alternative Therapeutic Vulnerabilities in Castration-Resistant Prostate Cancer. *Cell Rep* 2018;22(9):2236–45 doi 10.1016/j.celrep.2018.02.011. [PubMed: 29490263]
24. Han X, Wang C, Qin C, Xiang W, Fernandez-Salas E, Yang CY, et al. Discovery of ARD-69 as a Highly Potent Proteolysis Targeting Chimera (PROTAC) Degradable of Androgen Receptor (AR) for the Treatment of Prostate Cancer. *J Med Chem* 2019;62(2):941–64 doi 10.1021/acs.jmedchem.8b01631. [PubMed: 30629437]
25. Larochelle S, Amat R, Glover-Cutter K, Sanso M, Zhang C, Allen JJ, et al. Cyclin-dependent kinase control of the initiation-to-elongation switch of RNA polymerase II. *Nat Struct Mol Biol* 2012;19(11):1108–15 doi 10.1038/nsmb.2399. [PubMed: 23064645]
26. Yu M, Yang W, Ni T, Tang Z, Nakadai T, Zhu J, et al. RNA polymerase II-associated factor 1 regulates the release and phosphorylation of paused RNA polymerase II. *Science* 2015;350(6266):1383–6 doi 10.1126/science.1253338. [PubMed: 26659056]
27. Mitsiades N, Sung CC, Schultz N, Danila DC, He B, Eedunuri VK, et al. Distinct patterns of dysregulated expression of enzymes involved in androgen synthesis and metabolism in metastatic

- prostate cancer tumors. *Cancer Res* 2012;72(23):6142–52 doi 10.1158/0008-5472.CAN-12-1335. [PubMed: 22971343]
28. Roy R, Adamczewski JP, Seroz T, Vermeulen W, Tassan JP, Schaeffer L, et al. The MO15 cell cycle kinase is associated with the TFIIH transcription-DNA repair factor. *Cell* 1994;79(6):1093–101. [PubMed: 8001135]
  29. Ramanathan Y, Rajpara SM, Reza SM, Lees E, Shuman S, Mathews MB, et al. Three RNA polymerase II carboxyl-terminal domain kinases display distinct substrate preferences. *J Biol Chem* 2001;276(14):10913–20 doi 10.1074/jbc.M010975200. [PubMed: 11278802]
  30. Larochelle S, Batliner J, Gamble MJ, Barboza NM, Kraybill BC, Blethrow JD, et al. Dichotomous but stringent substrate selection by the dual-function Cdk7 complex revealed by chemical genetics. *Nat Struct Mol Biol* 2006;13(1):55–62 doi 10.1038/nsmb1028. [PubMed: 16327805]
  31. Sharma NL, Massie CE, Ramos-Montoya A, Zecchini V, Scott HE, Lamb AD, et al. The androgen receptor induces a distinct transcriptional program in castration-resistant prostate cancer in man. *Cancer Cell* 2013;23(1):35–47 doi 10.1016/j.ccr.2012.11.010. [PubMed: 23260764]
  32. Sharma A, Yeow WS, Ertel A, Coleman I, Clegg N, Thangavel C, et al. The retinoblastoma tumor suppressor controls androgen signaling and human prostate cancer progression. *J Clin Invest* 2010;120(12):4478–92 doi 10.1172/JCI44239. [PubMed: 21099110]
  33. Tomlins SA, Rhodes DR, Perner S, Dhanasekaran SM, Mehra R, Sun XW, et al. Recurrent fusion of TMPRSS2 and ETS transcription factor genes in prostate cancer. *Science* 2005;310(5748):644–8 doi 10.1126/science.1117679. [PubMed: 16254181]
  34. Wang X, Qiao Y, Asangani IA, Ateeq B, Poliakov A, Cieslik M, et al. Development of Peptidomimetic Inhibitors of the ERG Gene Fusion Product in Prostate Cancer. *Cancer Cell* 2017;31(4):532–48 e7 doi 10.1016/j.ccell.2017.02.017. [PubMed: 28344039]
  35. Chymkowitz P, Le May N, Charneau P, Compe E, Egly JM. The phosphorylation of the androgen receptor by TFIIH directs the ubiquitin/proteasome process. *EMBO J* 2011;30(3):468–79 doi 10.1038/emboj.2010.337. [PubMed: 21157430]
  36. Tran C, Ouk S, Clegg NJ, Chen Y, Watson PA, Arora V, et al. Development of a second-generation antiandrogen for treatment of advanced prostate cancer. *Science* 2009;324(5928):787–90 doi 10.1126/science.1168175. [PubMed: 19359544]
  37. Watson PA, Arora VK, Sawyers CL. Emerging mechanisms of resistance to androgen receptor inhibitors in prostate cancer. *Nat Rev Cancer* 2015;15(12):701–11 doi 10.1038/nrc4016. [PubMed: 26563462]
  38. O'Connor CM, Perl A, Leonard D, Sangodkar J, Narla G. Therapeutic targeting of PP2A. *Int J Biochem Cell Biol* 2018;96:182–93 doi 10.1016/j.biocel.2017.10.008. [PubMed: 29107183]
  39. Bhardwaj A, Singh S, Srivastava SK, Honkanen RE, Reed E, Singh AP. Modulation of protein phosphatase 2A activity alters androgen-independent growth of prostate cancer cells: therapeutic implications. *Mol Cancer Ther* 2011;10(5):720–31 doi 10.1158/1535-7163.MCT-10-1096. [PubMed: 21393425]
  40. Korenchuk S, Lehr JE, L MC, Lee YG, Whitney S, Vessella R, et al. VCaP, a cell-based model system of human prostate cancer. *In Vivo* 2001;15(2):163–8. [PubMed: 11317522]
  41. Kita Y, Goto T, Akamatsu S, Yamasaki T, Inoue T, Ogawa O, et al. Castration-Resistant Prostate Cancer Refractory to Second-Generation Androgen Receptor Axis-Targeted Agents: Opportunities and Challenges. *Cancers (Basel)* 2018;10(10) doi 10.3390/cancers10100345.
  42. Sabari BR, Dall'Agnese A, Boija A, Klein IA, Coffey EL, Shrinivas K, et al. Coactivator condensation at super-enhancers links phase separation and gene control. *Science* 2018;361(6400) doi 10.1126/science.aar3958.
  43. Boija A, Klein IA, Sabari BR, Dall'Agnese A, Coffey EL, Zamudio AV, et al. Transcription Factors Activate Genes through the Phase-Separation Capacity of Their Activation Domains. *Cell* 2018;175(7):1842–55 e16 doi 10.1016/j.cell.2018.10.042. [PubMed: 30449618]
  44. Lolli G, Johnson LN. CAK-Cyclin-dependent Activating Kinase: a key kinase in cell cycle control and a target for drugs? *Cell Cycle* 2005;4(4):572–7. [PubMed: 15876871]
  45. Larochelle S, Chen J, Knights R, Pandur J, Morcillo P, Erdjument-Bromage H, et al. T-loop phosphorylation stabilizes the CDK7-cyclin H-MAT1 complex in vivo and regulates its CTD

kinase activity. *EMBO J* 2001;20(14):3749–59 doi 10.1093/emboj/20.14.3749. [PubMed: 11447116]

46. Chipumuro E, Marco E, Christensen CL, Kwiatkowski N, Zhang T, Hatheway CM, et al. CDK7 inhibition suppresses super-enhancer-linked oncogenic transcription in MYCN-driven cancer. *Cell* 2014;159(5):1126–39 doi 10.1016/j.cell.2014.10.024. [PubMed: 25416950]
47. Christensen CL, Kwiatkowski N, Abraham BJ, Carretero J, Al-Shahrour F, Zhang T, et al. Targeting transcriptional addictions in small cell lung cancer with a covalent CDK7 inhibitor. *Cancer Cell* 2014;26(6):909–22 doi 10.1016/j.ccell.2014.10.019. [PubMed: 25490451]
48. Wang Y, Zhang T, Kwiatkowski N, Abraham BJ, Lee TI, Xie S, et al. CDK7-dependent transcriptional addiction in triple-negative breast cancer. *Cell* 2015;163(1):174–86 doi 10.1016/j.cell.2015.08.063. [PubMed: 26406377]
49. Stein MN, Goodin S, Dipaola RS. Abiraterone in prostate cancer: a new angle to an old problem. *Clin Cancer Res* 2012;18(7):1848–54 doi 10.1158/1078-0432.CCR-11-1805 1078–0432.CCR-11-1805 [pii]. [PubMed: 22451619]
50. Reid AH, Attard G, Danila DC, Oommen NB, Olmos D, Fong PC, et al. Significant and sustained antitumor activity in post-docetaxel, castration-resistant prostate cancer with the CYP17 inhibitor abiraterone acetate. *J Clin Oncol* 2010;28(9):1489–95 doi 10.1200/JCO.2009.24.6819 JCO.2009.24.6819 [pii]. [PubMed: 20159823]
51. Mukherji D, Pezaro CJ, De-Bono JS. MDV3100 for the treatment of prostate cancer. *Expert Opin Investig Drugs* 2012;21(2):227–33 doi 10.1517/13543784.2012.651125.
52. Arora VK, Schenkein E, Murali R, Subudhi SK, Wongvipat J, Balbas MD, et al. Glucocorticoid receptor confers resistance to antiandrogens by bypassing androgen receptor blockade. *Cell* 2013;155(6):1309–22 doi 10.1016/j.cell.2013.11.012 S0092–8674(13)01425–6 [pii]. [PubMed: 24315100]
53. Korpai M, Korn JM, Gao X, Rakiec DP, Ruddy DA, Doshi S, et al. An F876L Mutation in Androgen Receptor Confers Genetic and Phenotypic Resistance to MDV3100 (Enzalutamide). *Cancer Discov* 2013;3(9):1030–43 doi 10.1158/2159-8290.CD-13-0142 2159–8290.CD-13-0142 [pii]. [PubMed: 23842682]
54. Chen W, Rogatsky I, Garabedian MJ. MED14 and MED1 differentially regulate target-specific gene activation by the glucocorticoid receptor. *Mol Endocrinol* 2006;20(3):560–72 doi 10.1210/me.2005-0318. [PubMed: 16239257]
55. Liu Z, Merkurjev D, Yang F, Li W, Oh S, Friedman MJ, et al. Enhancer activation requires trans-recruitment of a mega transcription factor complex. *Cell* 2014;159(2):358–73 doi 10.1016/j.cell.2014.08.027. [PubMed: 25303530]
56. Li Q, Deng Q, Chao HP, Liu X, Lu Y, Lin K, et al. Linking prostate cancer cell AR heterogeneity to distinct castration and enzalutamide responses. *Nature communications* 2018;9(1):3600 doi 10.1038/s41467-018-06067-7.
57. Asangani IA, Wilder-Romans K, Dommeti VL, Krishnamurthy PM, Apel II, Escara-Wilke J, et al. BET Bromodomain Inhibitors Enhance Efficacy and Disrupt Resistance to AR Antagonists in the Treatment of Prostate Cancer. *Mol Cancer Res* 2016;14(4):324–31 doi 10.1158/1541-7786.MCR-15-0472. [PubMed: 26792867]
58. Kinoshita E, Kinoshita-Kikuta E, Koike T. Separation and detection of large phosphoproteins using Phos-tag SDS-PAGE. *Nat Protoc* 2009;4(10):1513–21 doi 10.1038/nprot.2009.154. [PubMed: 19798084]



**Statement of Significance**

Potent inhibition of AR signalling is critical to treat castration-resistant prostate cancer. This study uncovers a driver role for CDK7 in regulating AR-mediated transcription through phosphorylation of MED1, thus revealing a therapeutically targetable potential vulnerability in AR-addicted CRPC.

Author Manuscript

Author Manuscript

Author Manuscript

Author Manuscript

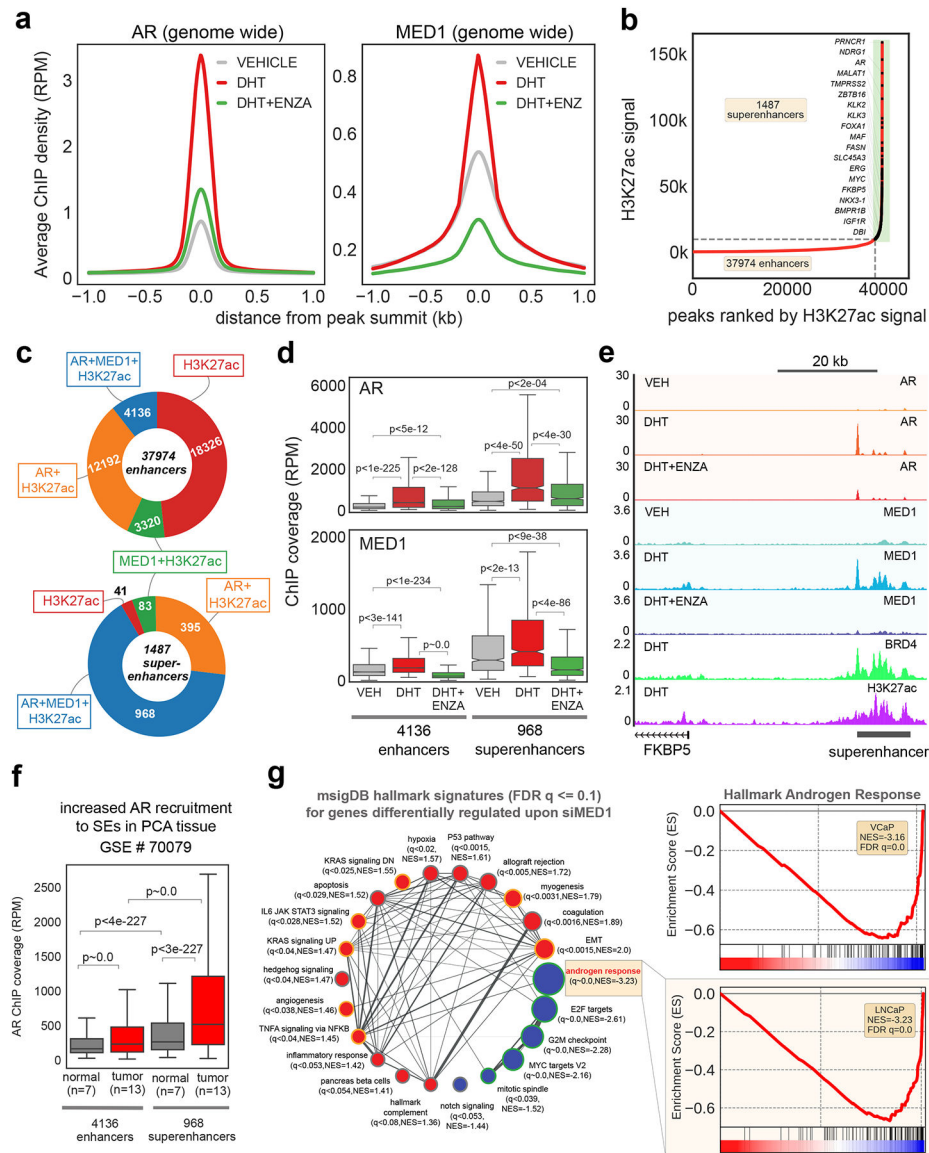


**Figure 1** | . MED1 undergoes phosphorylation upon androgen stimulation and is recruited to AR bound super-enhancers.

(a) AR activation increases MED1 recruitment to the chromatin. Genome-wide averaged AR and MED1 ChIP-seq enrichment in VCaP cells grown in steroid-deprived charcoal striped serum (CSS) containing media for 3 days, followed by 12h stimulation with 10 nM DHT or DHT plus 5  $\mu$ M enzalutamide. (b) Rank ordered H3K27ac ChIP-seq signal showing the presence of enhancers and super-enhancer (SE) regions in VCaP cells. (c) Preferential binding of MED1 to the AR bound SE. Pie chart displaying the overlap of H3K27ac enhancers and SE with AR and/or MED1 peaks. (d) Anti-androgen reverses MED1 binding to SE. Normalized enrichment of AR and MED1 in the enhancers and SE in the presence of DHT and/or ENZA in VCaP cells. (e) Genome browser view of AR, MED1, BRD4, and H3K27ac ChIP-Seq data at the *FKBP5* locus. The SE region is depicted with a black bar on the bottom right. (f) Increased AR recruitment to the SE in the PCa tumors compared to normal tissues. Box plot showing AR enrichment signal in the enhancer and SE regions in 7

normal and 13 tumor samples. (g) *MED1* knockdown blocks AR-mediated transcription. RNA-seq followed by Gene-Set Enrichment Analysis (GSEA) showing the various hallmark signatures up- (red) and down-regulated (blue) upon *MED1* knockdown. The inset shows the negative enrichment of the Hallmark androgen response signature in *MED1* knockdown VCaP and LNCaP cells.

Author Manuscript

Author Manuscript

Author Manuscript

Author Manuscript

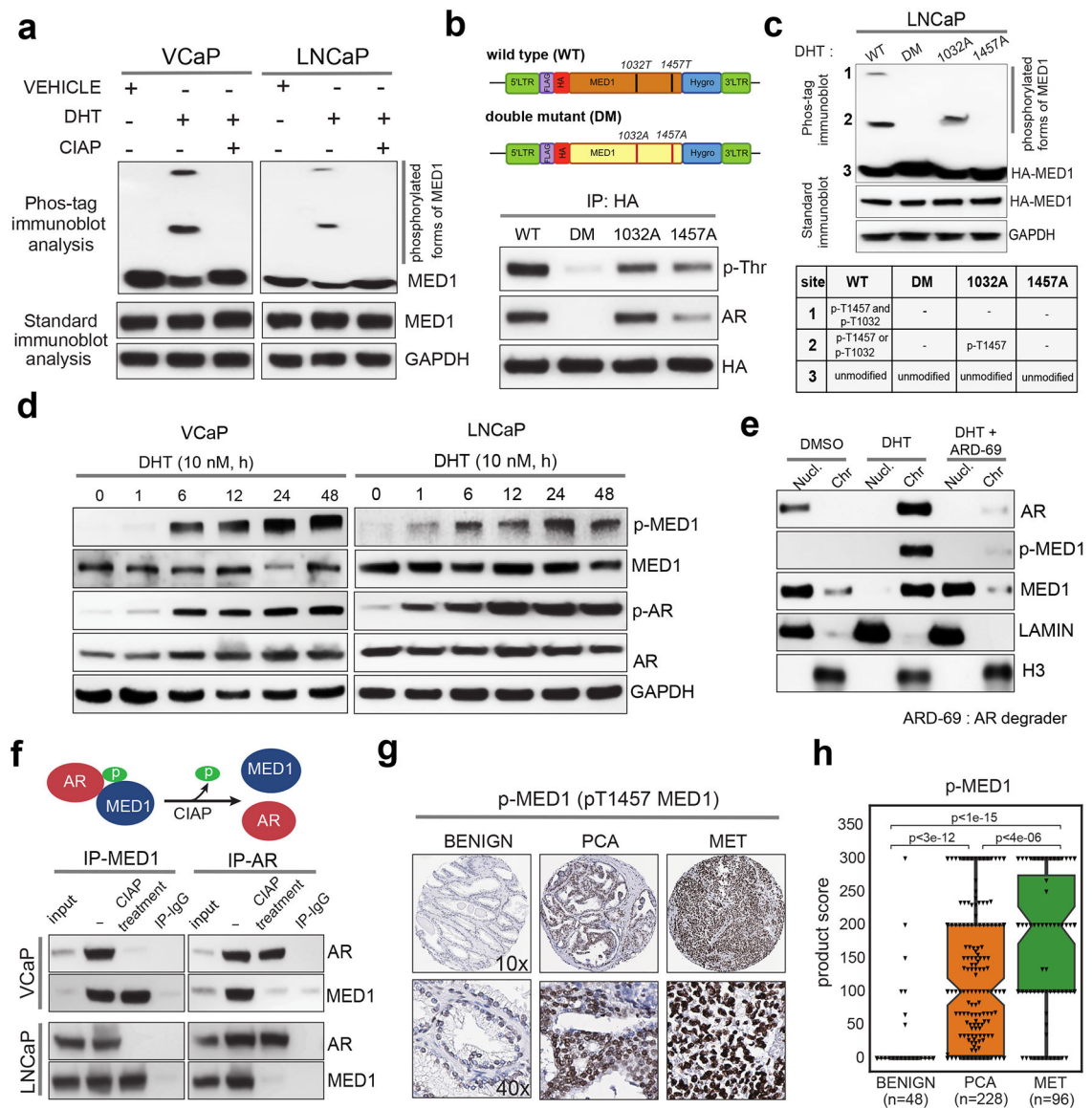


**Figure 2 | . MED1 undergoes phosphorylation upon androgen stimulation and is recruited to AR bound enhancers and super-enhancers.**

(a) MED1 phosphorylation upon activation of AR signaling. Cells were stimulated with DHT, and nuclear fractions were treated with or without calf intestine alkaline phosphatase (CIAP) before Phos-tag SDS-PAGE and immunoblotting for MED1. Control immunoblots were done on normal gels with the indicated antibodies. (b) *Top*, Illustration of the FLAG/HA-tagged wild-type (WT) MED1 and threonine-phosphorylation site T1032A/T1457A double-mutant (DM) MED1. *Bottom*, Immunoprecipitation of HA-tagged WT MED1, single and double mutant MED1 in LNCaP cells. Whole cell lysates were immunoprecipitated with anti-HA antibody followed by immunoblot analyses using anti-phospho-threonine and anti-AR antibody. (c) LNCaP Cells grown in CSS containing media were transfected with HA-tagged wild-type (WT), double mutant (DM), T1032A or T1457A mutant MED1 plasmids for 48h followed by stimulation with DHT for 12h. The nuclear proteins were extracted and used for Phos-tag SDS-PAGE and standard immunoblotting

with HA antibody. The table below indicates the identity of bands present on the phos-tag blot. (d) Immunoblot analyses showing time dependent increase in p-MED1 (p-T1457 MED1) levels by DHT stimulation in VCaP and LNCaP cells. (e) Chromatin and soluble nuclear fractions extracted from LNCaP cells grown in CSS containing media for 48h and subsequent stimulation with DHT alone for 12h or DHT for 6h followed by 6h treatment with ARD-69 (100 nM) were used to probe the indicated proteins. LAMIN and total H3 served as controls for nuclear and chromatin fractions respectively. (f) *Top*, Schematic depicting phosphorylation dependent MED1-AR interaction. *Bottom*, LNCaP cells were starved and stimulated with DHT, the nuclear proteins obtained were employed for reciprocal co-immunoprecipitation followed by immunoblotting with the indicated antibodies. (g, h) Tissue microarray analysis of p-MED1 in Benign, PCA (primary), and MET (metastatic) prostate tissues and quantification of their product scores.

Author Manuscript

Author Manuscript

Author Manuscript

Author Manuscript



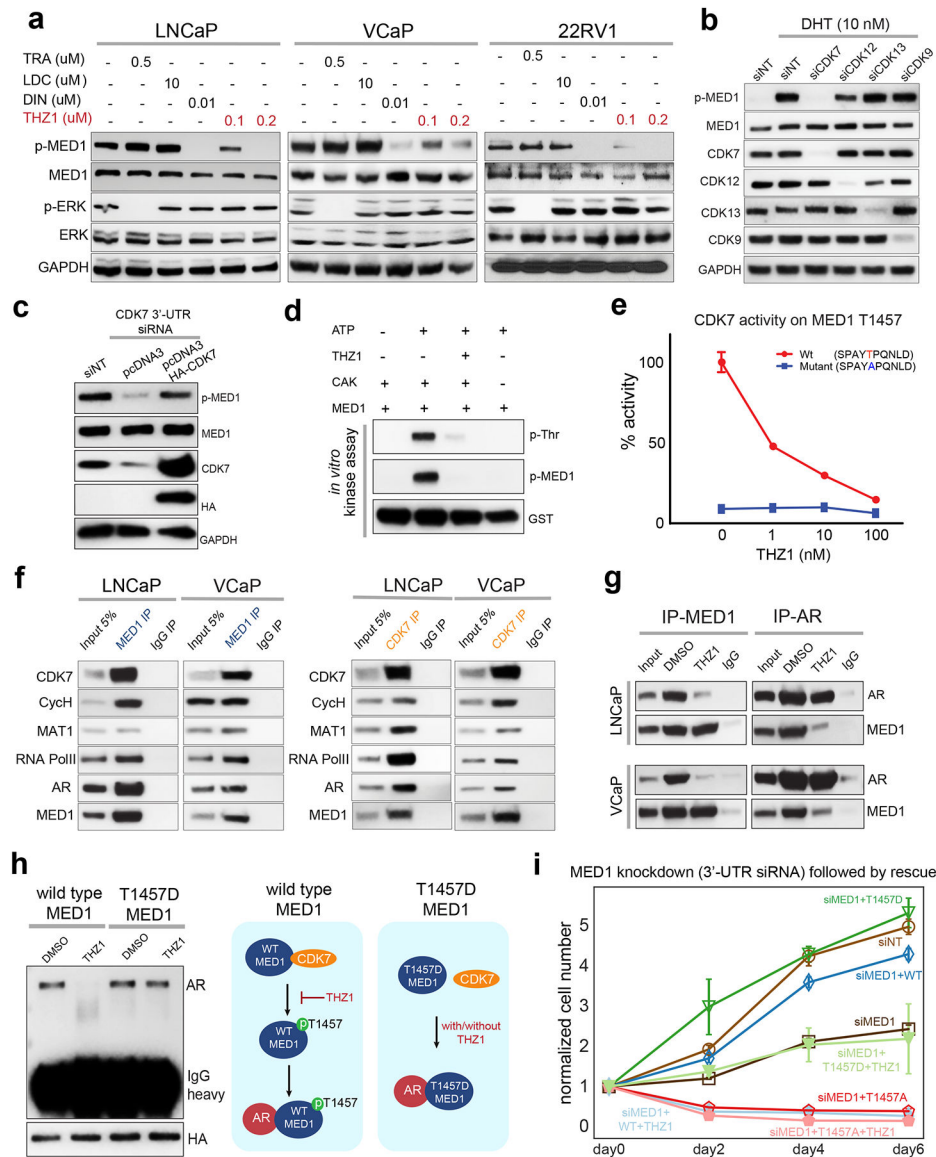


**Figure 3 | . CDK7 phosphorylation of MED1 at T1457 is essential for AR-MED1 interactions.** (a) THZ1 blocks MED1 phosphorylation. Immunoblot analysis showing the levels of the indicated proteins in PCa cell lines treated with DMSO or TRA (trametinib–MEK inhibitor), LDC000067 (CDK-9 inhibitor), DIN (Dinaciclib–panCDK inhibitor), THZ1 (CDK7/12/13 inhibitor) for 24h. p-ERK was used as positive control for TRA. (b) Knockdown of *CDK7* affects DHT-induced p-MED1. Proteins extracted from LNCaP cells transfected with indicated siRNA and grown in CSS containing media for 48h followed by treatment with vehicle or 10 nM DHT for 12h were used. (c) CDK7 overexpression rescue *CDK7* knockdown effect on MED1 phosphorylation. Total proteins extracted from LNCaP cells transfected with 3'-UTR targeting siRNA against *CDK7* along with vector control or HA-CDK7 plasmid for 72h was subjected to immunoblotting for the indicated target. (d) CDK7 phosphorylates MED1 in vitro. Kinase reaction mixtures containing CAK complex and GST-tagged MED1 protein (aa1391–1490) was prepared as indicated. After 60 min incubation at

30°C, the reaction mixtures were subjected to immunoblot analysis with the indicated antibody. (e) Luminescence based kinase assay showing CDK7 activity on WT vs T1457A mutant peptide and its response to varying concentration of THZ1. (f) Reciprocal co-IP analysis using nuclear lysates from LNCaP and VCaP cells with MED1 and CDK7 specific antibodies, demonstrating the interaction between MED1 and CDK7 in the transcriptional complex consisting of cyclinH, MAT1, RNA PolII and AR. (g) THZ1 treatment leads to disruption of MED1-AR interaction. IP followed by immunoblotting, using nuclear extracts from cells treated with DMSO or 100 nM THZ1 for 6h. (h) *Left*, T1457D phosphomimic interacts with AR even in the presence of THZ1. Nuclear extracts from LNCaP cells engineered to express HA-tagged MED1 WT or T1457D phosphomimic and treated with 100 nM THZ1 for 12h were subjected to immunoprecipitation with HA antibody followed by immunoblotting for AR. HA served as input control. *Right*, schematic depicting the phosphorylation-dependent interaction of MED1 and AR, and the effect of THZ1. (i) T1457D expressing cells demonstrate resistance to THZ1. LNCaP cells were co-transfected with control or siRNA targeting *MED1* 3'-UTR along with WT, T1457A or T1457D constructs. 48h post-transfection, equal number of cells were plated and treated with DMSO or 100 nM THZ1 and counted on indicated days (n=3). Also see supplementary figure 5d.

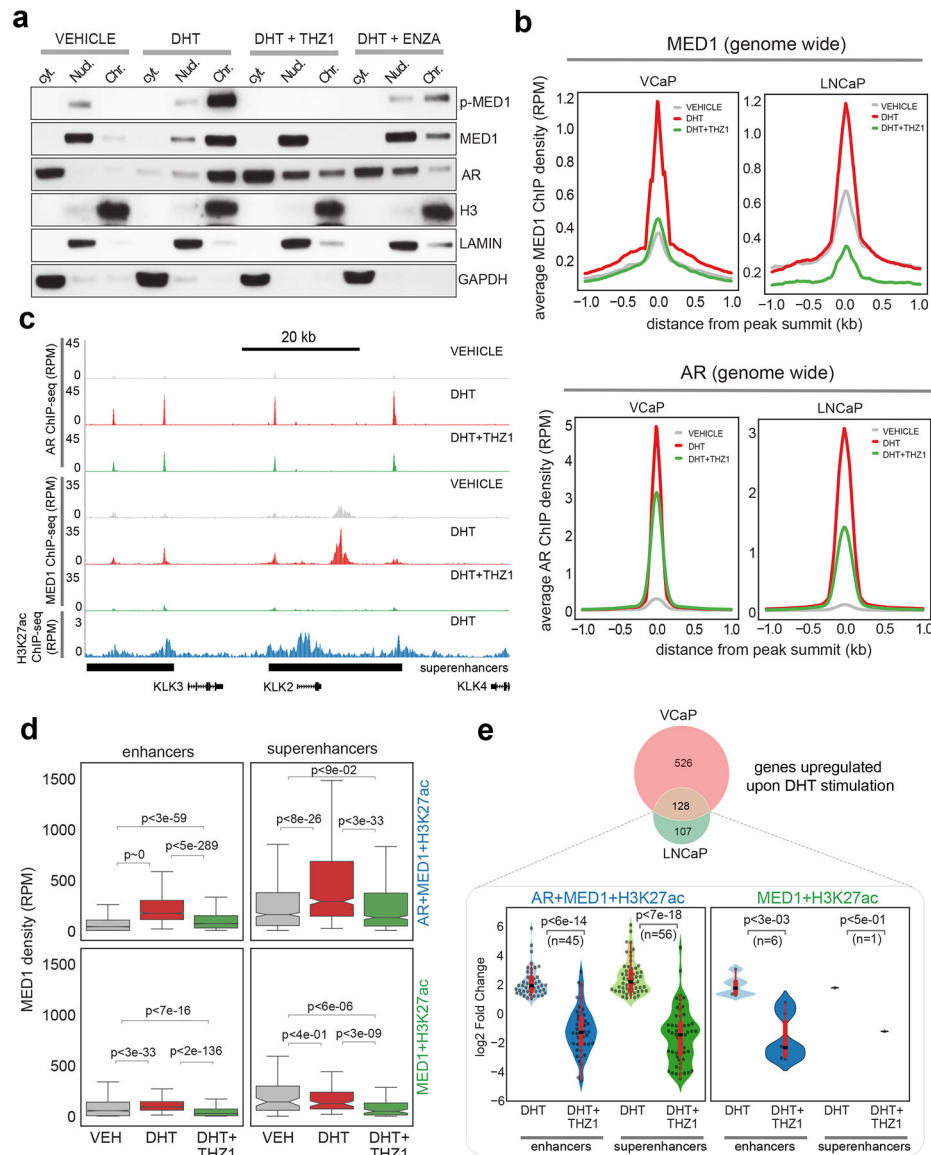


**Figure 4 | . CDK7 inhibition by THZ1 disrupts co-recruitment of MED1 and AR to the chromatin.**

(a) Immunoblot analysis demonstrating the loss of chromatin bound MED1 (p-MED1) upon THZ1 treatment. Chromatin, nuclear and cytoplasmic fractions from LNCaP cells grown in CSS containing media for 3-days following stimulation with DHT in the absence/presence of 100 nM THZ1 for 6h were used to probe the indicated proteins. Enzalutamide at 5  $\mu$ M was used as a direct anti-AR. (b) Genome-wide averaged MED1 and AR ChIP-seq enrichment in VCaP and LNCaP cells grown as in (a). (c) Genome browser tracks of AR, MED1, and H3K27ac binding at the KLK2, KLK3 and KLK4 locus in the indicated condition for VCaP. The super-enhancers (SEs) associated with this region are displayed as black bars at the bottom. (d) MED1 is recruited in a ligand-dependent manner to AR +MED1+H3K27ac regions. Box plots showing MED1 densities (RPM) at AR co-bound and the AR-devoid enhancers and SEs in vehicle, DHT and DHT+THZ1 treated samples. (e) Integrative analysis of RNA-seq and ChIP-seq shows majority of AR target genes associate

with AR+MED1 occupied enhancers and SE. (*Top*) Venn diagram showing 128 genes commonly upregulated upon DHT treatment in VCaP and LNCaP cells. (*Bottom*) Each of the 128 genes were associated with enhancers and SE regions described in (d) and the change in their expression under different treatment condition is shown as a violin plot. The significance values shown in panels (d) and (e) were computed using a two-tailed Student's t-test.

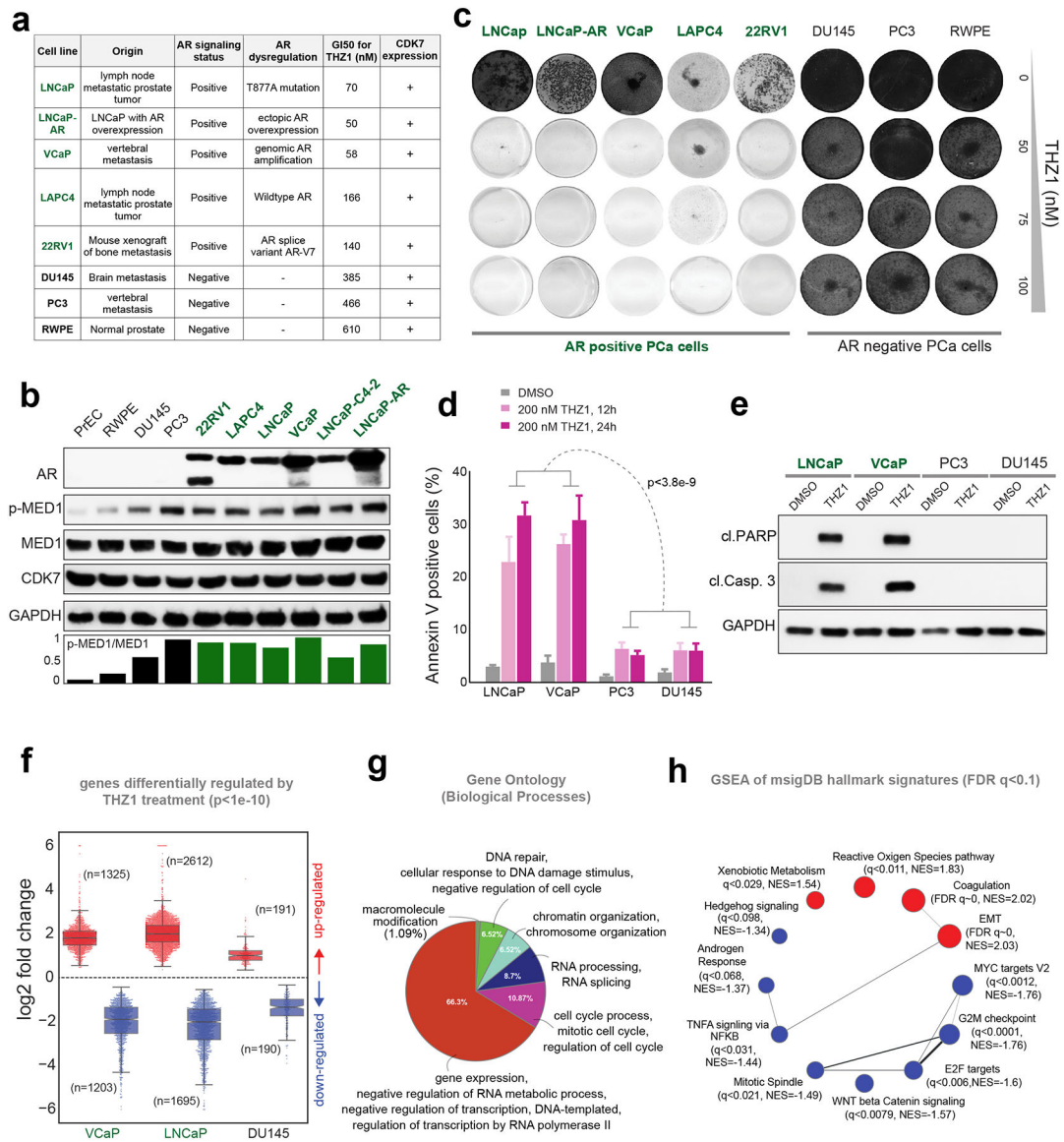


**Figure 5 | . Prostate cancer cells with active AR-signaling are sensitive to CDK7 inhibition.**

(a) GI50 for THZ1 in a panel of eight PCa cell lines is shown alongside their site of origin, AR status, AR dysregulation, and CDK7 expression. (b) Immunoblot analysis of AR, p-MED1, MED1, CDK7 in six AR positive and four AR negative PCa cell lines, GAPDH was used as the loading control. (c) Colony formation assays in the presence of THZ1. Cells were cultured in the presence or absence of THZ1 for 12–14 days followed by staining. (d) Annexin V-FITC staining showing percentage of apoptotic cells upon THZ1 treatment. Statistical significance was determined by two-tailed Student's t-test. (e) Immunoblot showing cleaved PARP and cleaved caspase-3 in PCa cells treated with 200 nM THZ1 for 24h. (f) Fold changes of differentially expressed genes determined by RNA-seq in three mCRPC cells treated with 100 nM THZ1 for 24h. (g) Gene Ontology (GO) terms for genes down-regulated, by at least 4-fold, upon THZ1 treatment in VCaP and LNCaP cells. (h) GSEA network plot showing positively (red) and negatively (blue) enriched hallmark



signature gene sets, as determined by GSEA with FDR  $q < 0.1$ , in THZ1 treated VCaP and LNCaP cells.

Author Manuscript

Author Manuscript

Author Manuscript

Author Manuscript

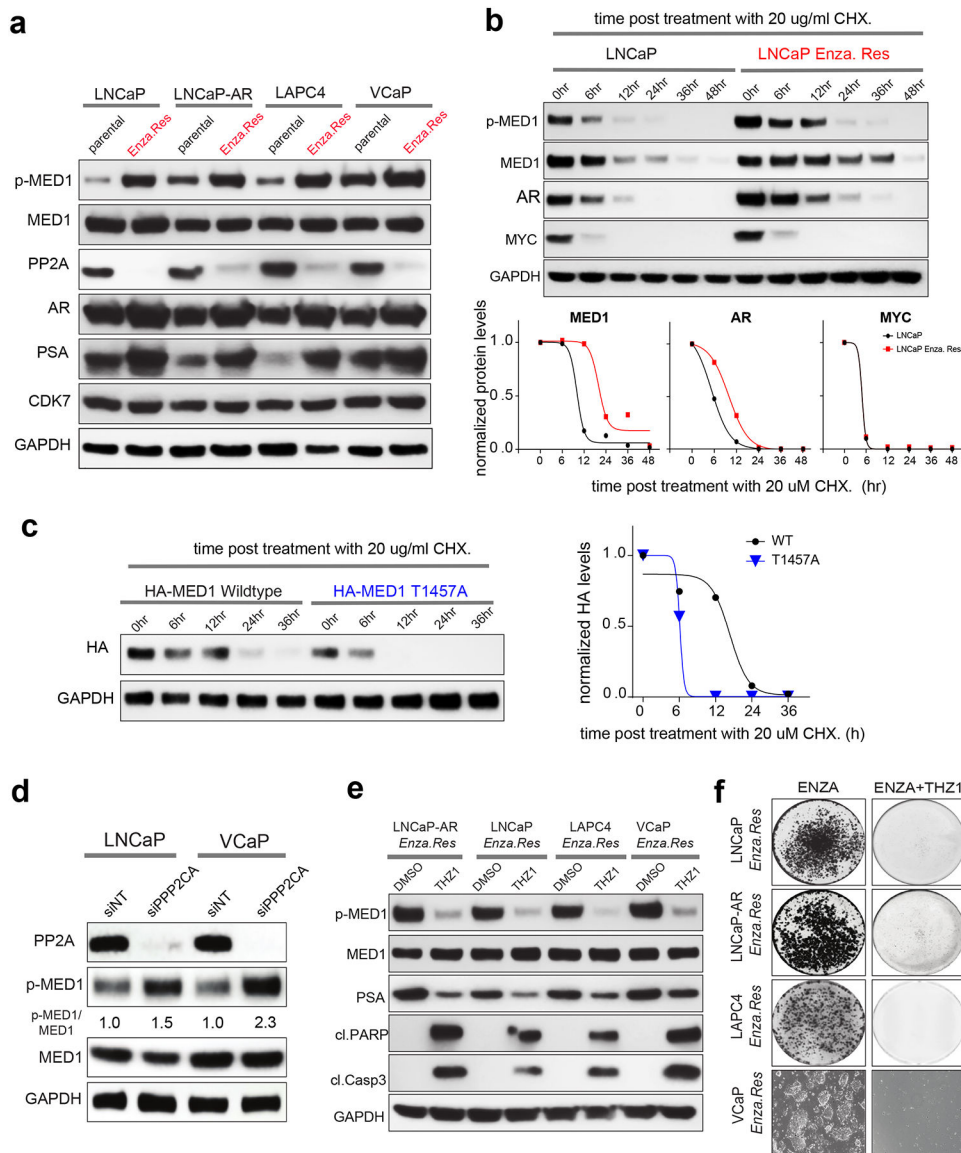


**Figure 6 | . Increased p-MED1 with a concomitant reduction in PP2A and sensitivity to THZ1 in enzalutamide resistant PCa cells.**

(a) Increased p-MED1 and reduced PP2A levels in AR driven Enzalutamide refractory PCa cells. Immunoblot analysis of indicated targets in four parental and enzalutamide resistant cell lines. (b) MED1 demonstrates increased stability in enzalutamide resistant cells. *Top panel*, immunoblot analysis of p-MED1, MED1, AR, and MYC in parental and enzalutamide resistant LNCaP derivative treated with 20 ug/ml cycloheximide as indicated. MYC - a rapidly translated and highly labile protein was used as a control for cycloheximide treatment. GAPDH served as a loading control. *Bottom panel*, graph showing normalized band intensities determined using ImageJ. (c) T1457A mutation decreases MED1 stability. *Left*, Protein extracts from LNCaP cells transfected with HA-tagged WT or phospho-dead T1457A mutant and treated with cycloheximide for varying time-points were subjected to immunoblotting with HA antibody. *Right*, graph showing GAPDH normalized band intensities. (d) Knockdown of *PPP2CA* – a catalytic unit of PP2A led to increase in p-MED1

expression in PCa cells. Immunoblot analysis of PP2A (PPP2CA), p-MED1 and MED1 in LNCaP and VCaP cells 72h post-transfection with siNT or siRNA targeting *PPP2CA*. The ratio of p-MED1 to MED1 is indicated. GAPDH was used as a loading control. (e) Immunoblot analysis of p-MED1, MED1, PSA, cleaved PARP, cleaved caspase-3 in the four-enzalutamide resistant PCa cell lines treated with vehicle or 200 nM THZ1 for 24h. (f) Colony formation assays in the enzalutamide resistant PCa cell lines under enzalutamide alone or in combination with 50 nM THZ1 treatment for 14 days followed by staining

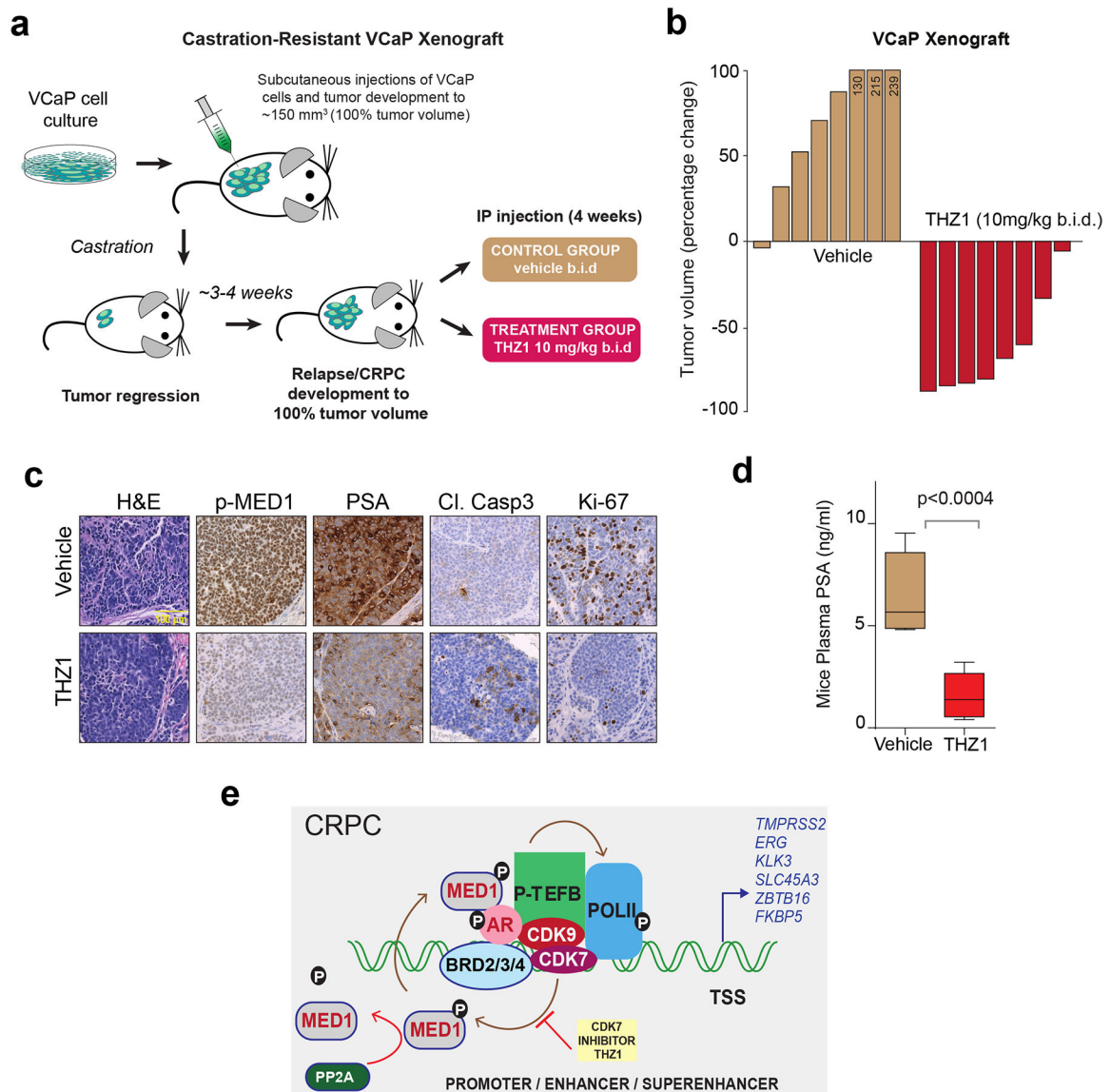


**Figure 7 | . THZ1 blocks CRPC growth *in vivo*.**

(a) Schematic illustrating the VCaP CRPC mouse xenograft experimental design. (b) Castrated mice bearing VCaP CRPC xenograft received vehicle-D5W (n=8) or 10mg/kg THZ1 (n=8) twice daily for 4 weeks. The percent change in volume for each tumor after 28 days of treatment is shown as a waterfall plot (y axis). (c) Representative images of H&E, p-MED1, PSA, Cl.Caspase3, and KI-67 immunohistochemistry staining of THZ1 or vehicle treated VCaP CRPC xenograft tumors. (d) Plasma PSA levels in vehicle and THZ1 treated mice. P-values were computed using two-tailed student's t-test. (e) Proposed model of the mechanism of action of CDK7 inhibition in AR-addicted CRPC.